Mechanisms for Quasi-Stationary Behavior in Simulated Heavy-Rain-Producing Convective Systems

RUSS S. SCHUMACHER

Department of Atmospheric Science, Colorado State University, Fort Collins, and National Center for Atmospheric Research, Boulder, Colorado*

(Manuscript received 11 June 2008, in final form 19 November 2008)

ABSTRACT

In this study, idealized numerical simulations are used to identify the processes responsible for initiating, organizing, and maintaining quasi-stationary convective systems that produce locally extreme rainfall amounts. Of particular interest are those convective systems that have been observed to occur near mesoscale convective vortices (MCVs) and other midlevel circulations. To simulate the lifting associated with such circulations, a low-level momentum forcing is applied to an initial state that is representative of observed extreme rain events. The initial vertical wind profile includes a sharp reversal of the vertical wind shear with height, indicative of observed low-level jets.

Deep moist convection initiates within the region of mesoscale lifting, and the resulting convective system replicates many of the features of observed systems. The low-level thermodynamic environment is nearly saturated, which is not conducive to the production of a strong surface cold pool; yet the convection quickly organizes into a back-building line. It is shown that a nearly stationary convectively generated low-level gravity wave is responsible for the linear organization, which continues for several hours. New convective cells repeatedly form on the southwest end of the line and move to the northeast, resulting in large local rainfall amounts. In the later stages of the simulated convective system, a cold pool does develop, but its interaction with the strong reverse shear at low levels is not optimized for the maintenance of deep convection along its edge. A series of sensitivity experiments shows some of the effects of hydrometeor evaporation and melting, planetary rotation, and the imposed mesoscale forcing.

1. Introduction

Deep moist convection often organizes into clusters or lines that are much larger than the size of individual updrafts; these organized groups of clouds are known collectively as mesoscale convective systems (MCSs; Houze 2004). The organization and motion characteristics of MCSs determine the overall distribution of rainfall. Fast-moving MCSs may produce relatively small precipitation totals over a large geographic area; the rainfall from such MCSs is vital to agriculture in the central United States (e.g., Fritsch et al. 1986; Ashley et al. 2003). On the other hand, MCSs that move slowly can result in extremely large rainfall amounts over a small area and can cause life-threatening flash floods (e.g., Chappell 1986; Doswell et al. 1996). Schumacher and Johnson (2005) identified the patterns of MCS organization that most often produce extreme local rainfall. One of these patterns, termed back-building/quasi-stationary (BB), consists of a line or cluster of deep convection in which new cells form upstream of their predecessors such that the system as a whole remains nearly stationary. This results in the repeated passage of heavy-rain-producing convective cells over locations along the line, a process often referred to as echo training.

In many cases, back-building MCSs occur along preexisting boundaries, such as outflows from previous convection [as in the simulation of Miller (1978) and the mesohigh flash flood type of Maddox et al. (1979)]. In other cases, however, convection initiates and organizes into this pattern with no apparent surface boundaries in the vicinity. Schumacher and Johnson (2009; hereafter SJ09) identified six such cases, all of which occurred

* The National Center for Atmospheric Research is sponsored by the National Science Foundation.

Corresponding author address: Dr. Russ Schumacher, NCAR, P.O. Box 3000, Boulder, CO 80307.
E-mail: rschumac@ucar.edu

DOI: 10.1175/2008JAS2856.1

near a midlevel cyclonic vorticity maximum, such as a mesoscale convective vortex (MCV). In all of these cases, a low-level jet (LLJ) interacted with the midlevel circulation, leading to lifting, destabilization, and convection initiation and organization just south of the vorticity center. All of these MCSs produced more than 200 mm (7.9 in) of rain in less than 12 h and led to destructive flash flooding. This study is aimed at understanding, through the use of idealized numerical simulations, the processes that initiate, organize, and maintain extreme-rain-producing MCSs such as these.

SJ09 found that quasi-stationary MCSs occurring near midlevel circulations typically form in environments with high relative humidity (RH) that are not conducive to the production of strong convectively generated cold pools. Cold pools are typically the cause for linear organization in MCSs (e.g., Rotunno et al. 1988; Parker and Johnson 2004), but MCSs driven by strong cold pools often have fast forward propagation speeds. Here, we seek to understand how convective systems become linearly organized and move slowly. In a case study of an extreme-rain-producing MCS, Schumacher and Johnson (2008, hereafter SJ08) found that a nearly stationary low-level gravity wave, rather than a cold pool, was responsible for the observed linear organization. This study will attempt to reach more general conclusions about quasi-stationary MCSs by examining the behavior of convection in an environment representative of observed cases but without the unique attributes of each event.

Another important feature in the convective environments discussed by SJ09 is the lifting and destabilization that result from the interaction between an LLJ and a midlevel circulation. Isentropic upglide on the downshear side of MCVs was discussed by Raymond and Jiang (1990), and Trier et al. (2000) showed how this upward motion can lift layers of conditionally unstable air to saturation, resulting in increased convective available potential energy, decreased convective inhibition, and moist absolutely unstable layers (MAULs; Bryan and Fritsch 2000). All of these factors make the environment more favorable for additional convective development on the downshear side of a midlevel vortex, and recent observations have confirmed that these are important processes in midlatitude MCVs (Davis and Trier 2007; Trier and Davis 2007). Fritsch et al. (1994) discussed how the reversal of vertical wind shear with height associated with an LLJ creates a scenario in which the ambient shear above the LLJ opposes the direction of the mean flow and the convective systems that form near MCVs in this environment move very slowly.

To simulate quasi-stationary convective systems that occur near midlevel circulations in an idealized framework, we take an approach similar to that of Dudhia and Moncrieff (1987), Crook and Moncrieff (1988, hereafter CM88), and Loftus et al. (2008, hereafter LWD08). These investigators simulated the initiation and maintenance of convection that occurs within large-scale lifting; they were not specifically concerned with MCVs, but MCVs and other midlevel circulations represent another application of their ideas. Herein, we build on their results by applying a momentum forcing (lifting) to simulations that include three dimensions and other important aspects such as ice microphysics. We will demonstrate that these results are faithful simulations of the types of convective systems that develop in environments with mesoscale to synoptic-scale lifting, such as those that occur near MCVs or other midlevel circulations.

2. Description of the numerical model and experimental design

For the simulations presented herein, version 1.11 of the nonhydrostatic cloud model described by Bryan and Fritsch (2002) was used. These three-dimensional simulations used a composite thermodynamic sounding (Fig. 1), which was calculated from the inflow environment of six extreme rain events described in SJ09, to create a horizontally homogeneous base state. The wind profile used in the model is very similar to the composite profile, but the surface winds are slightly stronger, as are the zonal winds between 10 and 14 km; these fields are averaged, smoothed wind fields from the case-study simulation in SJ08 (Fig. 2). A slight upper-level jet streak was present in that case, which was less prominent in the composite. The sensitivity to this feature was tested and found to not cause any significant differences in the results to be presented here. This wind profile was used primarily because near-surface rapid update cycle (RUC; Benjamin et al. 2004) analyses underestimated the observed surface winds in MCS inflow regions in some cases. The primary feature of this wind profile is the strong reversal of shear associated with the LLJ, illustrated by the hairpin shape on a wind hodograph (Fig. 1). In these simulations, this LLJ only exists in the vertical; there is no initial horizontal variation in the wind, except for that associated with the forcing described below. In this study, only results from simulations using this particular wind profile are included. The sensitivity to changes in the wind profile has been considered initially in Schumacher (2008) and is currently under further investigation, with the results to be presented in a future manuscript.

To initiate deep moist convection in the model, a momentum forcing based on the work of LWD08 is

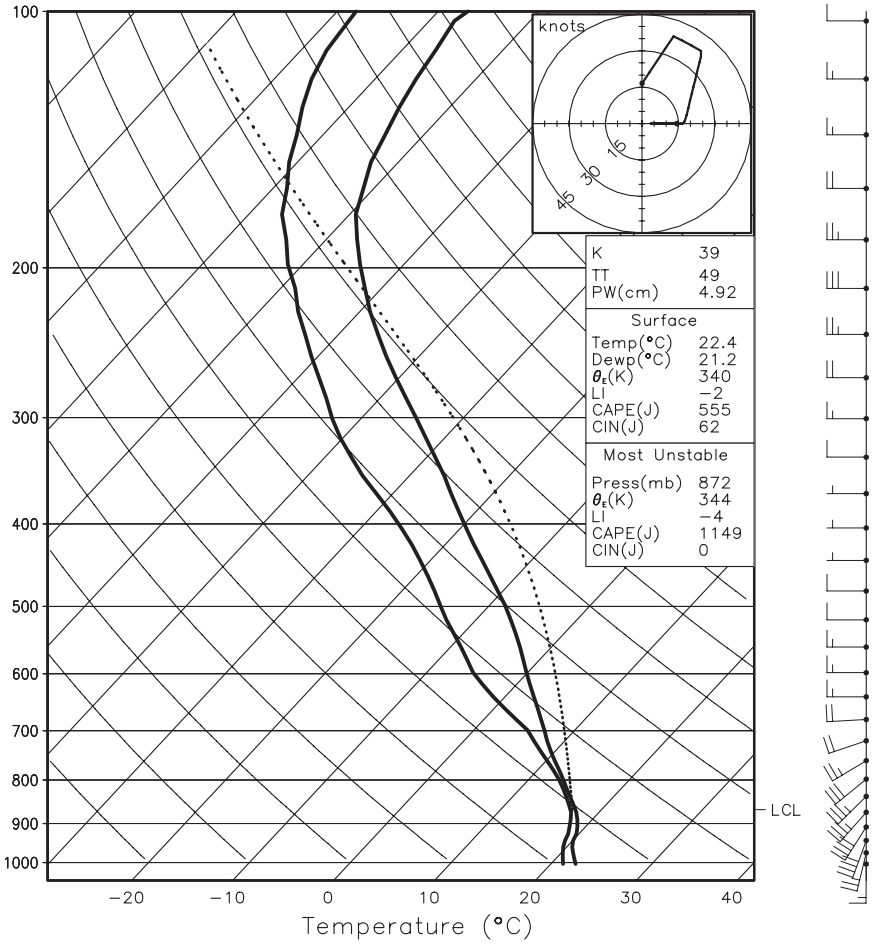

FIG. 1. Skew T–log$p$ diagram showing the sounding used to initialize the horizontally homogeneous base state. The thermodynamic sounding is a composite sounding from six extreme rain events that occurred near midlevel circulations (described in SJ09). The wind profile is similar to the composite wind profile; see the text and Fig. 2 for more information. The parcel path for the parcel with the highest θ_e in the lowest 3 km is shown by the dotted line.

used. This method has been chosen so that it is possible to simulate the mesoscale to synoptic-scale lifting that takes place with MCVs and other midlevel circulations in shear, while avoiding the additional complexities of vortex dynamics. Examining the interactions between midlevel vortices and strong low-level shear is an avenue of potential future research, but the primary focus of this study is on the workings of the MCSs. The discussion to follow will demonstrate that a momentum forcing is a reasonable method for simulating the lifting that occurs with midlevel circulations in shear and for initiating simulated convective systems that resemble the observed MCSs shown in SJ09.

A full description of the momentum forcing, including relevant equations, can be found in LWD08. A few important modifications were made for this study, which are outlined below. In this method for initiating convection, a convergence field is prescribed, and then the horizontal wind perturbations necessary to create that convergence field are calculated and added to the basic state wind. LWD08 used a linear function with convergence maximized at the surface for the vertical structure, but the convection in the observed MCSs shown by SJ09 typically develops within elevated convergence and lifting. As such, a wave-shaped vertical structure (with only 1/2 vertical wavelength) is used here to create an elevated convergence maximum: $f(z) = \cos^2[(1/2)\pi\beta]$, where $\beta = |(z - z_c)/z_r|$, z_c is the height of the center of the imposed convergence field and z_r is its vertical scale.

The other notable difference from the method used in LWD08 is in the time-dependent application of the wind perturbations. LWD08 calculated the wind perturbations required to create a desired convergence field and then

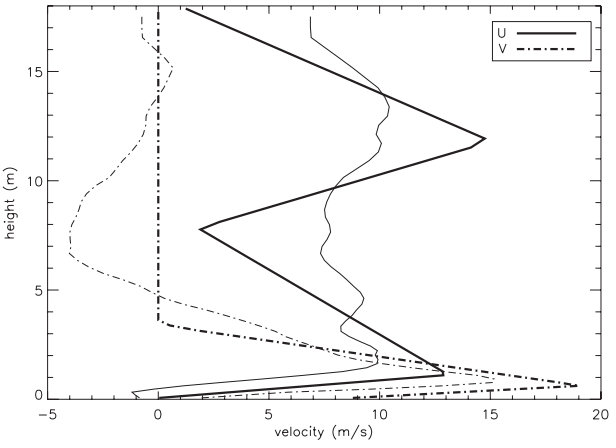

FIG. 2. Vertical wind profile used for the horizontally homogeneous initial state in the idealized simulations (thick lines). This is an averaged, smoothed wind profile from 0600 UTC in the case-study simulation presented in SJ08. The wind profile from the RUC composite is shown in the thin lines for comparison.

applied those same perturbations at each model time step. Thus, convergence was held constant, and any convectively generated effects on the wind field were neglected. This was appropriate for their investigation of the development of isolated multicellular convection over short periods of time. However, the goal in this study is to examine the important processes in organized MCSs, and the feedbacks between organized convection and the larger environment cannot be ignored. Therefore, rather than applying a constant convergence, the convergence starts at zero and is allowed to increase during the first few hours of the simulation. This amounts to a momentum forcing, similar to the approach used by CM88.[1] To create the forcing, we choose a maximum convergence value and calculate the associated wind perturbations, but then only add a fraction of those perturbations to the base-state wind at each time step. This allows the convergence field and associated vertical motions to gradually develop, while also allowing the flow that develops to feed back on the horizontal wind field. In all of the simulations presented here, the wind perturbations were positioned at the center of the model domain. Then the model domain was translated with a speed of $u = 7.5\ \mathrm{m\ s^{-1}}$ and $v = 2.5\ \mathrm{m\ s^{-1}}$, which was similar to the translation speed of the composite vortex shown in SJ09 (their Fig. 4). This method is essentially simulating a moving low-level forcing (such as an MCV) and how convection behaves when it develops within this forcing.

[1] As will be shown later in section 4b, continued forcing after the initiation of convection is not necessary to maintain a long-lived convective system.

TABLE 1. Parameters chosen for the convergence forcing in the idealized numerical simulations. Notation is as in LWD08; a brief description of the terms is provided in the table.

Domain size	$400 \times 400 \times 18.3$ km
x_c,y_c (horizontal center points of forcing)	200 km
λ_x,λ_y (shape control parameters)	70 km
z_c (vertical center point)	1.4 km
z_r (vertical radius)	1.0 km
$D_{\max}$ (maximum divergence)	$-1 \times 10^{-4}\ \mathrm{s^{-1}}$

The values of the parameters chosen for the momentum forcing are shown in Table 1. The shape control parameters, which determine the size and ellipticity of the convergence region, are much larger than those used in LWD08, as is the model domain; these were chosen to approximate the size of the convergence regions in the RUC analyses in observed cases. Appropriate values for the fraction of the wind perturbations to apply at each time step were found using trial and error in dry simulations before applying them to simulations with moisture for the thermodynamic environment used here.

To illustrate the structure and evolution of the forcing, some results from a dry simulation are shown in Fig. 3. This simulation used 1-km horizontal grid spacing and a stretched vertical grid with 61 levels and grid spacing increasing from 100 m near the surface to 500 m at the model top. Figure 3a shows that the convergence and associated vertical motions increase fairly quickly in the first 2 h of the simulation and then level off beyond that time. After 6 h, an approximately circular convergence field exists at the center of the domain (Fig. 3b). The vertical structure (Fig. 3c) shows the response to the elevated convergence, with a region of weak descent near the surface and ascent above. The applied lifting also alters the potential temperature field; there is a slight cool perturbation near the surface on the south side of the forcing and a stronger cool perturbation above and to the north of the forcing. Thus, there is a slight upward slope to the isentropes for parcels approaching from the south in the 1.5–2.5-km AGL layer, which is where the most unstable air is located when moisture is added. This lifting resembles the isentropic upglide in a midlevel positive potential vorticity (PV) anomaly discussed by Raymond and Jiang (1990). Although the vertical velocities are weak and the change in the slope of the isentropes is also relatively minor, parcels within the southwesterly low-level flow at around 2 km AGL are displaced upward by approximately 250 m. In Fig. 3d, an averaged vertical profile of

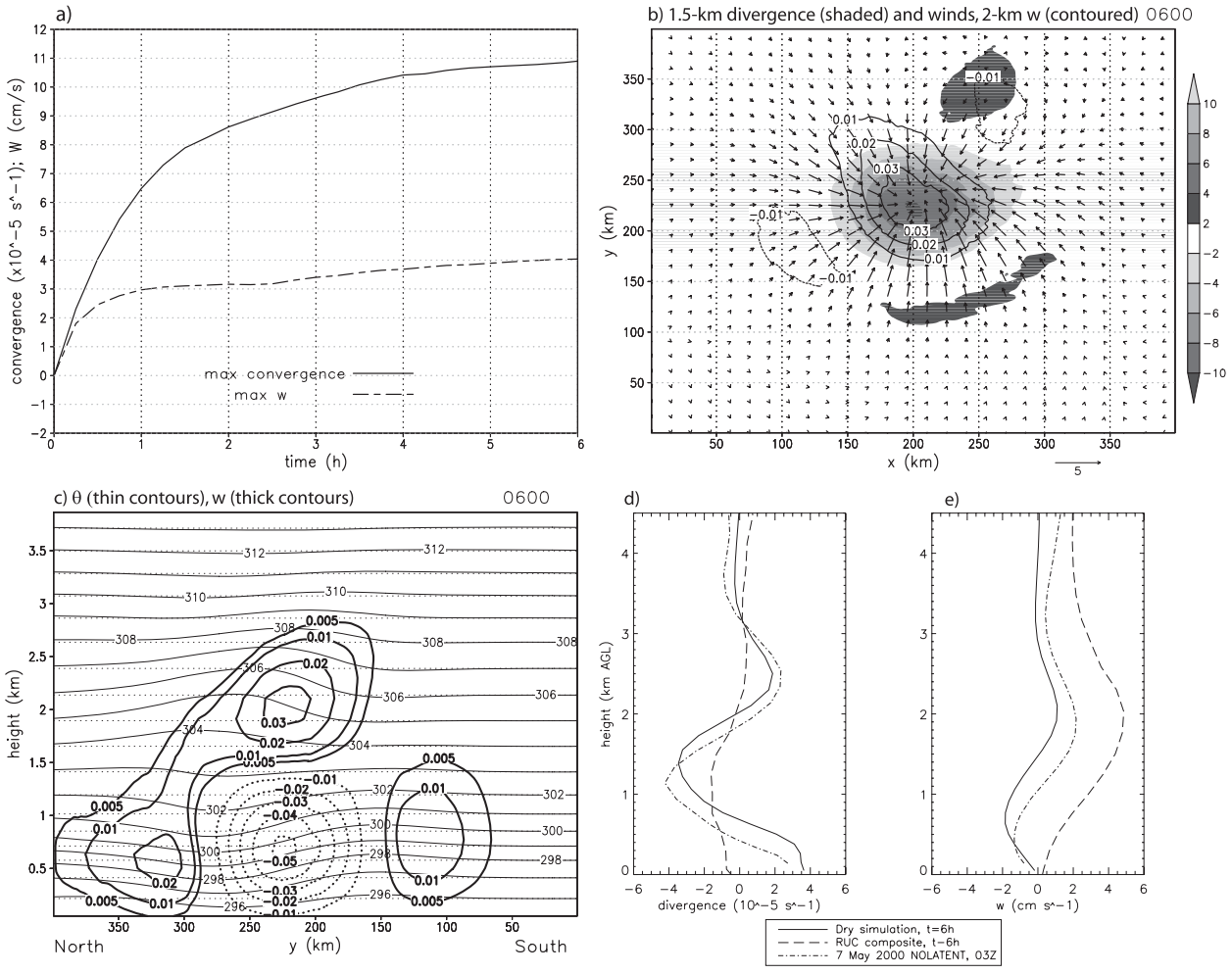

FIG. 3. (a) Time series showing the maximum convergence (solid line) and maximum upward vertical velocity (dashed line) in a dry simulation using the momentum forcing described in the text. For convergence, the units are 10^{-5} s^{-1} and for vertical velocity they are 10^{-2} m s^{-1}; both are plotted on the same axis. (b) Divergence (shaded every 2×10^{-5} s^{-1}) and wind perturbations (m s^{-1}; reference vector at bottom) at 1.5 km above the surface and vertical velocity (line contours every 0.01 m s^{-1}) at 2 km above the surface at $t = 6$ h in the dry simulation. (c) North–south vertical section of potential temperature and vertical velocity in the lowest 4 km of the dry simulation. The section is taken through the center of the domain, and values have been averaged over an area 20 km on either side of this line. The thin solid contours represent potential temperature at $t = 6$ h; the thin dashed contours show the potential temperature of the base state. Thick contours represent vertical velocity (m s^{-1}), with negative values dashed. (d) Vertical profiles of divergence (10^{-5} s^{-1}), averaged over a 150 km $\times$ 150 km box centered on the maximum convergence. The solid line is the divergence in the dry simulation after 6 h; the dashed line is from the RUC composites of SJ09 at 6 h before the heaviest rainfall; the dashed–dotted line is from the NOLATENT simulation of the 6–7 May 2000 case described in SJ08. (e) As in (d), but for vertical velocity (10^{-2} m s^{-1}).

the imposed convergence is compared with a similar profile from the RUC composite analysis in SJ09 and with a profile from the NOLATENT case-study simulation of SJ08, in which latent heating and cooling were neglected. The profile in the dry simulation compares very favorably with the NOLATENT simulation, which includes the full effects of an MCV but neglects moist convective processes. The shape of the profile in the RUC composite is also similar, although the convergence is weaker, which is likely a result of the coarser grid spacing in the RUC. Profiles of vertical velocity (Fig. 3e) also compare well with one another; the vertical motion in the RUC composite is stronger because it includes moist convective processes. In the dry simulation, the divergence and descent near the surface are fairly strong but, as will be shown, this does not prevent the initiation of deep convection in simulations with moisture.

The forcing applied in these simulations is slightly weaker than those used in similar past studies. The maximum vertical velocity here is just over 0.04 m s^{-1}, which is similar to the 0.05 m s^{-1} value in the idealized

MCV simulation of Trier et al. (2000; cf. their Fig. 5). The upward motion in CM88 approached 0.1 m s^{-1} (cf. their Fig. 4). Trier et al. (2000) reported upward displacements of over 800 m in 8 h, and the displacements shown in CM88 were approximately 300 m in 3 h, both of which are stronger than the value of 250 m in 6 h obtained using the method described above. In this context, it appears to be a justifiable method for initiating and maintaining a convective system that is similar to those observed to occur beneath midlevel circulations, without adding the complexities of the circulation itself.

The primary simulation to be presented below used horizontal grid spacing of 1 km and the same vertical grid spacing as the dry simulation. This grid spacing is not fully sufficient to resolve individual convective cells, but convective systems are well resolved (e.g., Weisman et al. 1997; Bryan et al. 2003). To better resolve convective motions, an additional simulation with $\Delta x = \Delta y = 500$ m was run. However, given the computing resources required for the 500-m simulation on a large domain, it was only run for 5 h, whereas the 1-km simulation was run for 11.5 h, and several sensitivity tests at $\Delta x = 1$ km were run for 9 h. Additionally, to speed up the initiation of convection in the 500-m run, a spectrum of random potential temperature perturbations with maximum magnitude of 2 K was applied at the initial time using the method of Bryan et al. (2007). In the 1-km run, convection was allowed to initiate naturally through the lifting process. The convection organizes more quickly in the 500-m run owing to the initial random convection, but the organization and evolution of the systems are otherwise very similar. Results from both simulations are shown where appropriate.

The model used herein has free-slip upper and lower boundaries, with a Rayleigh damping layer above 14 km. For the simulation with $\Delta x = 500$ m, the large time step is 3 s; for $\Delta x = 1$ km, $\Delta t = 5$ s. The model is configured to use sixth-order monotonic numerical diffusion (Knievel et al. 2007) and a positive-definite advection scheme such that moisture and scalar quantities are approximately conserved. It uses open-radiative lateral boundaries as formulated in Durran and Klemp (1983), and it restricts the outward flux of mass so that it does not exceed the total inward mass flux. This restriction was used because earlier attempts at simulating these types of MCSs showed unrealistic mass flux out of the boundaries and caused pressure falls throughout the domain. The model includes parameterized ice microphysics based on the scheme of Lin et al. (1983) and modified as described in Braun and Tao (2000). Radiative processes are neglected. In the primary simulation, the Coriolis force was neglected, but a sensitivity experiment that includes it will be discussed in section 4.

3. Results

a. Development and organization of convective system

As the lifting builds over the first few hours of the 1-km simulation, air near the center of the convergence zone is lifted to saturation, yielding a layer of cloudiness and moist absolute instability (Fig. 4a). The first deep convective cells appear in this region approximately 2.75 h into the simulation. As these cells develop, they create a low-level gravity wave signature, with cool perturbations indicating isentropes that have been displaced upward and warm perturbations denoting downward-displaced isentropes. This wave is similar to those shown in the idealized simulations of SJ08 (Fig. 4b, cf. their Fig. 22). SJ08 showed that in the same thermodynamic environment used here, one of the gravity wave modes excited by latent heating in convection has its maximum amplitude at approximately 1 km AGL. When these waves are excited within a wind field with a reversal of shear with height, the waves remain near their source rather than propagating away (see also Schmidt and Cotton 1990).

In time, the initially scattered deep convection (Fig. 5a) organizes into a quasi-linear arrangement, with new convection developing on the southwest flank (within the region of lifting) and deep convective cells moving from southwest to northeast along the line (Figs. 5b,c). The system attains this linear organization by $t = 3.5$ h in the 500-m simulation and by $t = 5.5$ h in the 1-km simulation. As the system began to organize, the convective line was initially organized parallel to the average deep-layer shear, but then between $t = 5.5$ h and $t = 7$ h it evolved such that the line had components both along and across the deep-layer shear vector (Fig. 5c). The organization and motion characteristics of this simulated system are very similar to those in observed extreme-rain-producing convective systems and are consistent with the BB pattern discussed by Schumacher and Johnson (2005). After approximately $t = 7.5$ h in the 1-km simulation, the convective line begins to surge southward (Figs. 5d,e); the processes leading to this surge at later times will be discussed in the next subsection.

The low-level potential temperature fields show that the initial linear organization is not caused by a cold pool. At $t = 6.75$ h, the primary area of convection is organized in a line from southwest to northeast, with a smaller region of developing convection to its west (Figs. 6a,b). At the surface, potential temperature perturbations θ' (calculated relative to the initial state) are generally weak beneath the most intense parts of the convective line (Fig. 6c). However, at 1 km AGL there is a strong signal of a wave, with narrow bands of warm

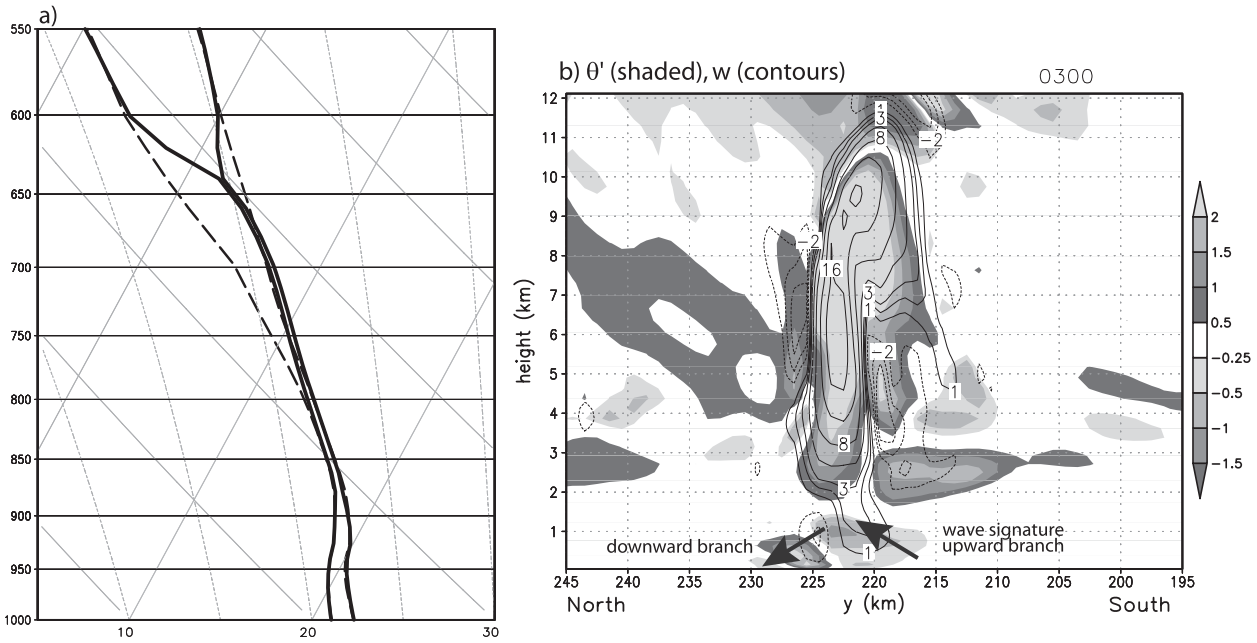

FIG. 4. (a) Skew T–log$p$ diagram showing the effect of the lifting on the environment. The initial thermodynamic profile is shown with the dashed lines, and the solid lines show the profile at $t = 1.75$ h at the center of the convergence zone. (b) North–south vertical cross section through one of the first deep convective cells at $t = 3$ h. Shown are potential temperature perturbations (K, shaded; see scale for scaling) and vertical velocity (contours at -4, -2, -1, 1, 2, 3, 5, 8, 12, and 16 m s^{-1}, with negative contours dashed).

and cool air existing beneath the two primary regions of deep convection (Fig. 6d). Where θ' is negative (positive), isentropes have been displaced upward (downward) from their initial state, and the narrow couplet seen in Fig. 6d extending northeastward from $x = 225$, $y = 225$ illustrates the presence of a wave pattern in the isentropes. Thus, rather than the low-level structure being defined by a density current as is the case with many linear MCSs, it is defined by a slow-moving gravity wave.

Because it was necessary to choose a size for the imposed region of lifting, the size of the resulting MCS is somewhat preordained by the size of the forcing. However, nothing about the momentum forcing favors linear organization for the resulting convection. The lack of a cold pool is to be expected, given that the nearly saturated low-level conditions inhibit the evaporation of raindrops. However, the tendency for convection to organize itself linearly without a cold pool is somewhat surprising. Interactions between the deep convection, a low-level gravity wave, and the vertical wind shear appear to be the organizing factors for this convective system.

An equivalent figure to Fig. 6 is shown in Fig. 7 for the simulation with 500-m grid spacing at $t = 5$ h. The features discussed above are also present in this run, and given the better resolution of convective motions at this grid spacing, the vertical structure of the convective system will be explored in the 500-m run. (The vertical structure in the 1-km run is qualitatively similar.) A vertical section through the convective line (Fig. 8a) reveals many similarities to those found in past observational and modeling studies (e.g., Houze et al. 1989; Fovell 2002). There is strong low-level inflow into a deep, nearly upright convective line, as well as an overturning circulation aloft (e.g., Thorpe et al. 1982). A broad region aloft has been warmed, which is a gravity wave response to the convective system's latent heating (e.g., Nicholls et al. 1991) and also reflects the transport of buoyant near-surface air upward by convection (e.g., Weisman 1992).

There are, however, several important differences between this system and most previously simulated MCSs, most notably the lack of a cold pool near the surface. For the purpose of comparison, a similar figure from a typical simulation of a cold-pool-driven squall line (Fovell and Tan 1998, their Fig. 1a) is included in Fig. 8b. In their simulation, there is strong low-level vertical motion along the edge of a cold pool with $\Delta\theta \approx -10$ K. They show that as air is lifted at the edge of the density current, new convective cells form periodically. The present simulation (Fig. 8a) also shows an updraft at low levels with periodic initiation of new cells (which will be discussed shortly), but the temperature structure is markedly different. There is no cold air near the surface on the north side of the updraft; instead,

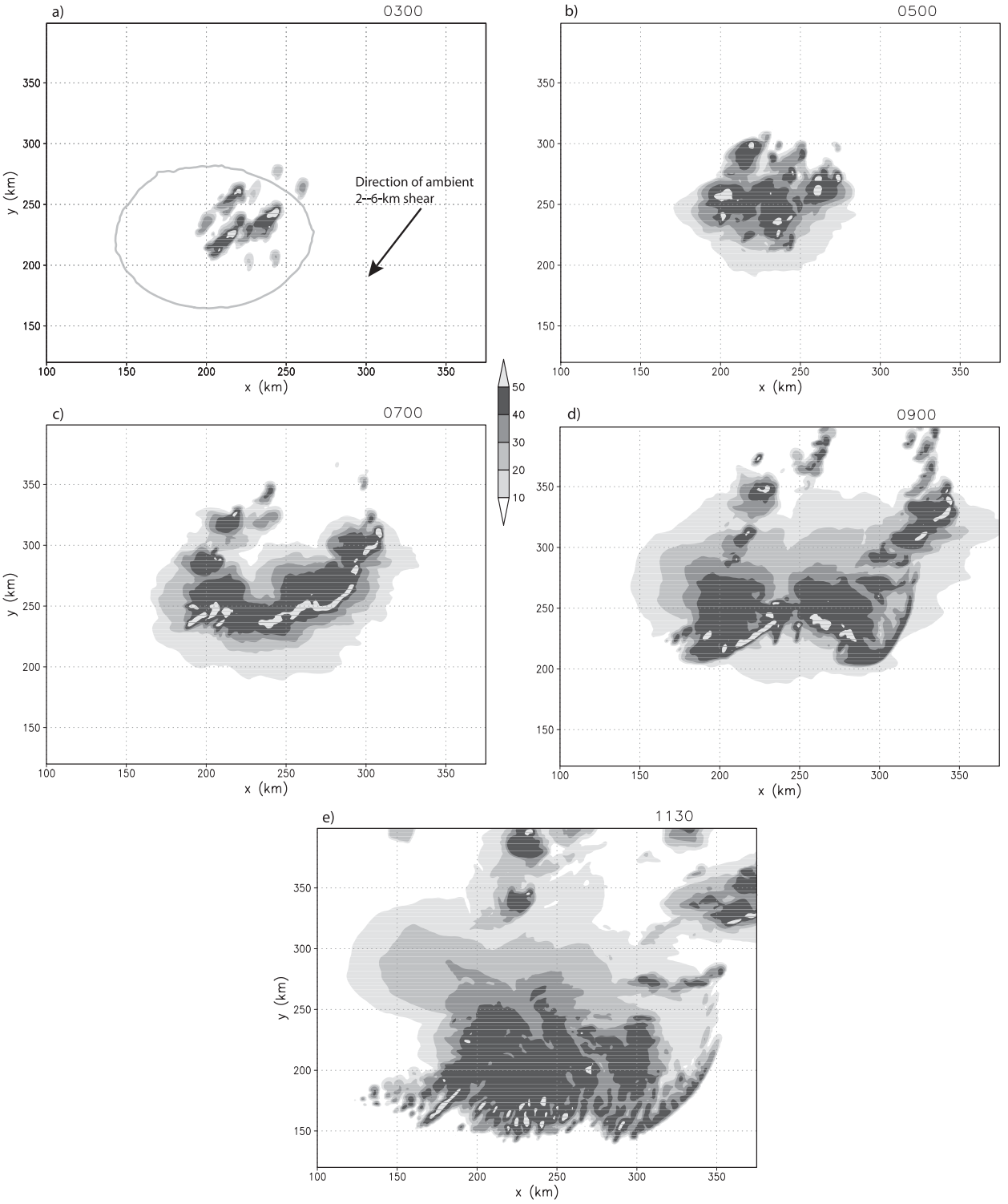

FIG. 5. Simulated composite radar reflectivity (dBZ) from the 1-km simulation at t = (a) 3, (b) 5, (c) 7, (d) 9, and (e) 11.5 h. The portion of the domain shown is the same in all panels; however, recall that the domain is being translated toward the east-northeast as discussed in the text. In (a), the -2×10^{-5} s^{-1} divergence contour from the dry simulation at t = 3 h and 1.5 km AGL (gray line) is included to illustrate the location of the imposed convergence. The direction of the ambient 2–6-km shear vector is also shown in (a).

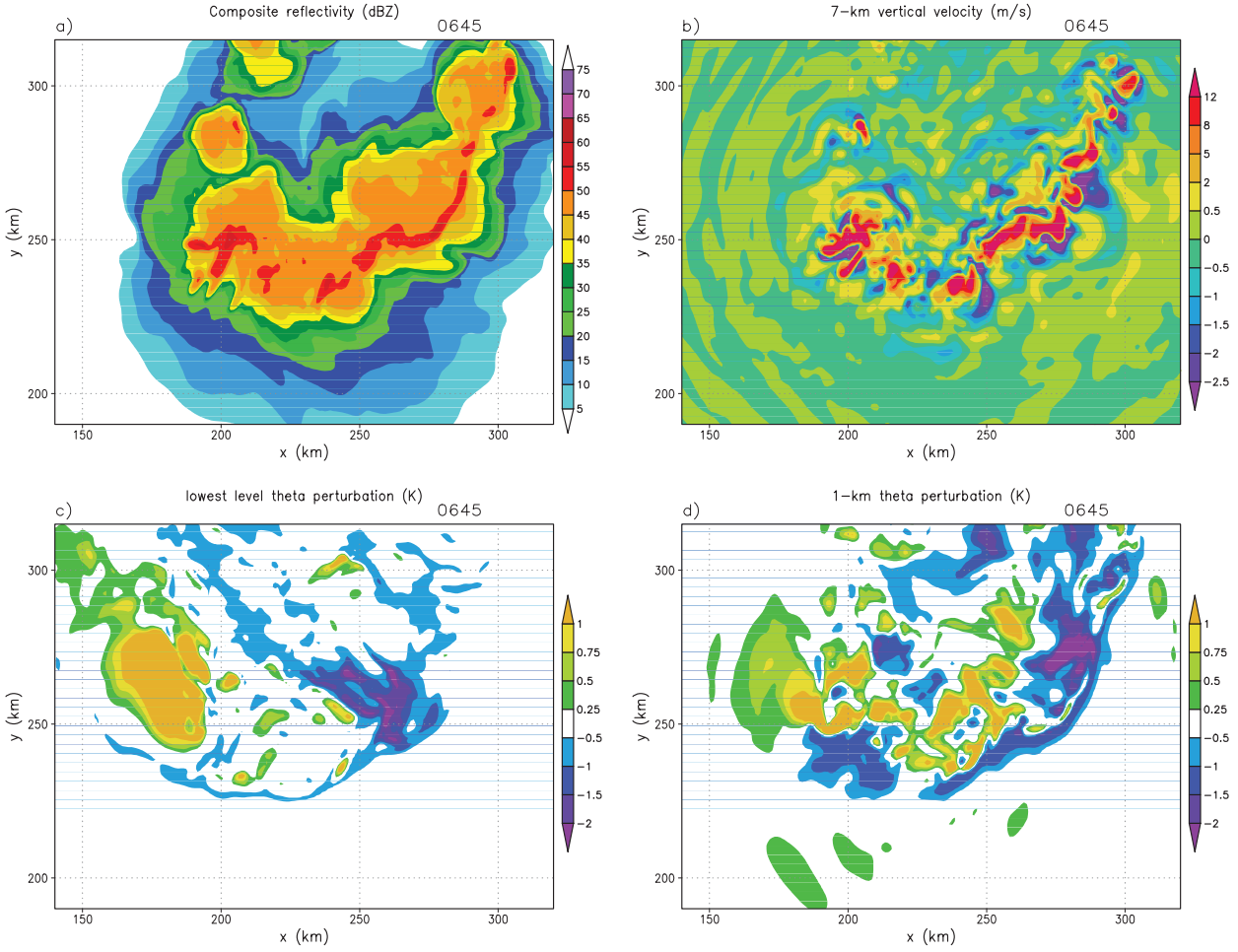

FIG. 6. (a) As in Fig. 5, but at $t = 6.75$ h and zoomed in on the region of deep convection. (b) Vertical velocity (m s^{-1}) at 7 km AGL at $t = 6.75$ h in the 1-km simulation. (c) Potential temperature perturbations (K) on the lowest model level at the same time. (d) Potential temperature perturbations at 1 km AGL.

there is an elevated cool perturbation almost directly below the updraft (e.g., at $z = 1$ km above $y = 190$–197 in Fig. 8a). Just to the north of the cool perturbation and updraft, there is a downdraft; this couplet is the vertical representation of the low-level gravity wave described above and shown in Fig. 7d.

To further differentiate the mechanisms for low-level lifting in this case from a density current, a vertical cross section showing the full buoyancy field (including hydrometeor loading effects) is shown in Fig. 9. The structures seen in Fig. 9 are generally similar to those in Fig. 8a, which only considers potential temperature perturbations, although some differences are also apparent. Most importantly, the signature of the low-level wave (indicated by the negatively buoyant air above $y = 195$) is still the predominant feature near where new convection is developing. This suggests that negative buoyancy caused by hydrometeor loading is not having a primary effect on the structure and development of the convective system.

Trajectories of air parcels originating at two different levels illustrate the effect of this gravity wave on the air that encounters it (Fig. 10a). Subsaturated air originating near the surface (i.e., in the lowest 500 m) approaches the wave from the south-southeast and is lifted sharply over the crest of the wave; then it just as quickly sinks on the other side. In contrast, parcels from within the elevated southwesterly inflow, which have already been destabilized by the large-scale lifting, are lifted over the wave, attain their level of free convection, and rise in deep updrafts. A closer look at the structure of the low-level wave reveals a distinct crest and trough in the isentropes (Fig. 10b). As near-surface parcels are lifted along the upward-sloping isentropes, they reach their lifting condensation level, clouds form, and the parcels continue to rise (Fig. 10b). However, the parcels then

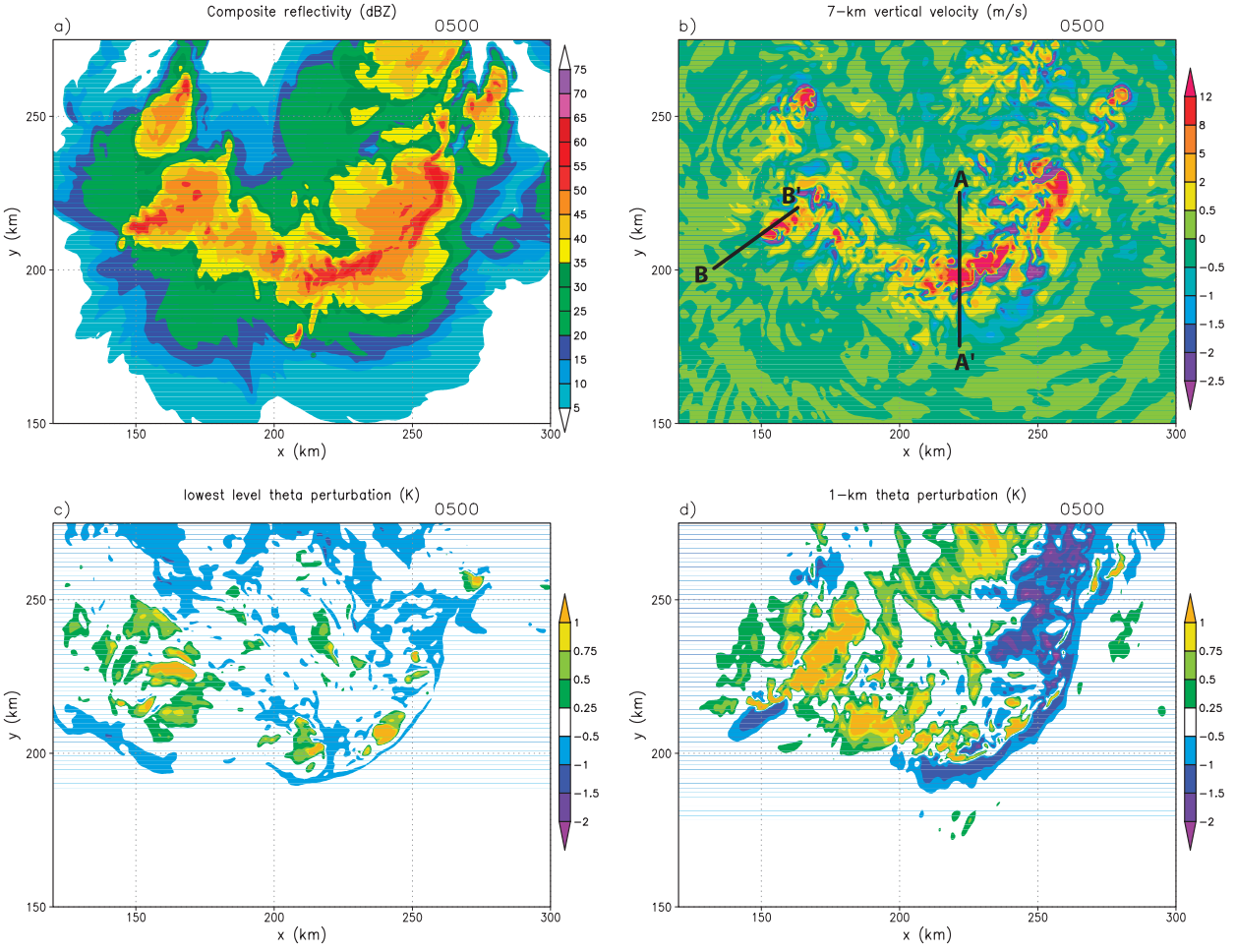

FIG. 7. As in Fig. 6, but for the 500-m simulation at $t = 5$ h. Lines A–A′ and B–B′ indicate the locations of vertical cross sections shown in Figs. 8–11.

move into the downward branch of the gravity wave, and they sink and become subsaturated once again.

The process of back-building is ubiquitous in the regions of deep convection in this simulation, and one location where it is very clearly illustrated is along the newly developing convective cluster to the west of the primary convective line (see line B–B′ in Fig. 7a). Figure 11 shows discrete cells forming upstream of their predecessors and developing into deep updrafts as they move northeastward, while the cluster is propagating toward the southwest. It also reveals the role of the low-level gravity wave in focusing the deep convection. At $t = 4.5$ h (Fig. 11a), a progression of convective cells is apparent: two deep, strong updrafts on the right (northeast) side of the figure, one strengthening cell to their southwest, and one relatively new updraft (referred to as cell number 1). Over the next 20 min (Figs. 11b,c), cell 1 develops into an intense updraft, and we see the initiation of cells 2 and 3 upstream. Cell 2 follows in the path of cell 1 and also becomes a deep updraft by $t = 5$ h (Fig. 11d), when another new cell (number 4) begins to appear. A similar multicellular back-building process is common to quasi-stationary convective systems [see, e.g., the schematic in Doswell et al. (1996, their Fig. 7)], but here the mechanism responsible for initiating new deep convective cells is not a traditional outflow boundary. Instead, as developing shallow updrafts encounter the low-level gravity wave, they are lifted and erupt into deep convective cells. (The wave is shown by the cool perturbations centered at approximately 1 km AGL in Fig. 11; the plane of the vertical section is parallel to the wave, so the wave appears as a long band of $\theta' < 0$.) Over the 30-min period shown in Fig. 11, the gravity wave (and associated convection) has also moved toward the southwest (i.e., it has propagated in the opposite direction of cell motion). When convection back-builds in this way and is linearly organized, it creates an optimal configuration for locally excessive rainfall amounts.

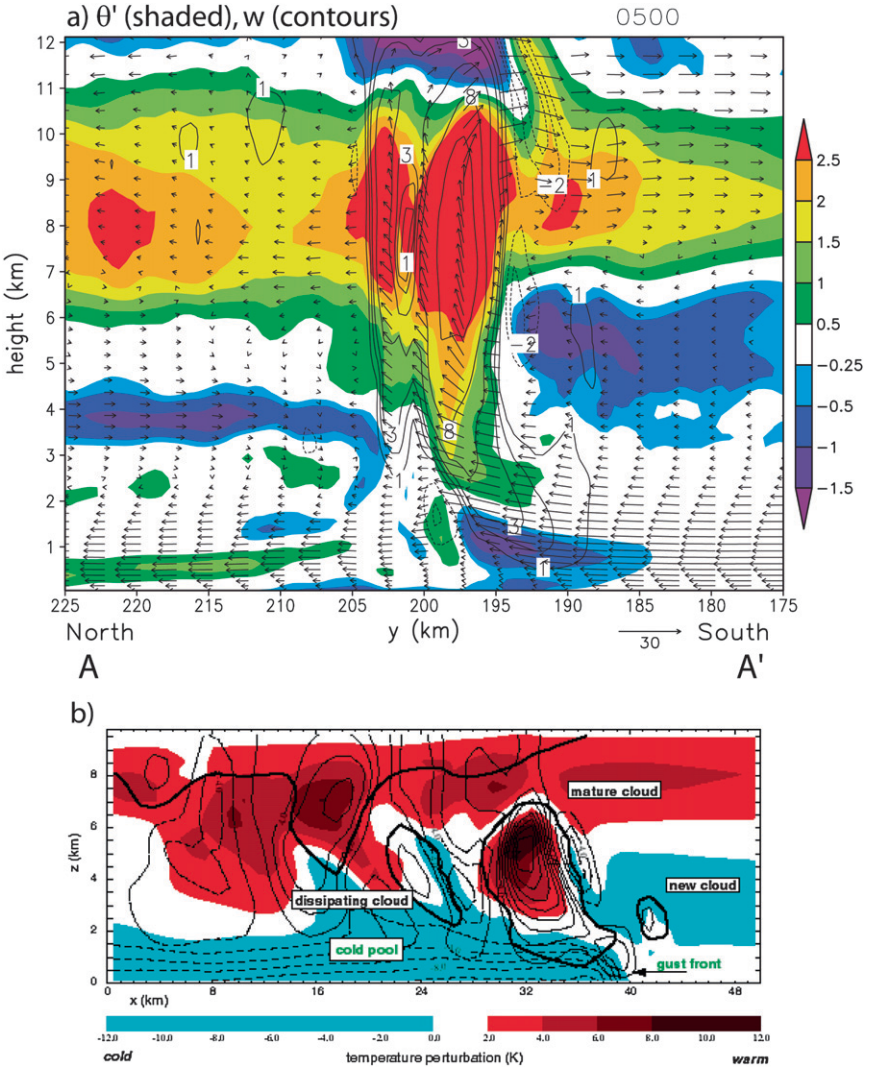

FIG. 8. (a) North–south vertical section through the convective line at $t = 5$ h in the 500-m simulation. The location of the cross section is shown by line A–A′ in Fig. 7b, and values have been averaged over an area 5 km on either side of this line. Shown are potential temperature perturbations (K; colors), vertical velocity (m s^{-1}; contoured as in Fig. 4), and system-relative, line-perpendicular flow vectors (m s^{-1}, shown at every fifth horizontal grid point). (b) A similar figure from Fovell and Tan (1998), showing a simulated cold-pool-driven squall line for comparison. The thin dashed contours near the surface are potential temperature perturbations, contoured every 2 K; note that these perturbations are significantly larger than those shown in (a). Color version of (b) used with permission from R. Fovell.

Although the discussion in the previous paragraph focused mainly on the immediate vicinity of the convection, the importance of the background lifting (which is meant to replicate forcing from a midlevel circulation) should not be neglected: it is what gets this process started initially, and it also aids in the initiation of the shallow cells upstream. In the case studied by SJ08, the shallow cells formed much farther upstream than they do in this simulation, but this was likely a result of inhomogeneities in the thermodynamic environment in that case that are not present here.

Most past research on linear convective systems has focused on the cold pool as an organization and maintenance mechanism because the environments in which most MCSs form have dry air at some level, which promotes evaporative cooling and cold-pool development. In this context, the above findings represent a much different mechanism for MCS organization and maintenance, although they are not entirely unique. The circumstances leading to the development of both gravity waves and density currents are considered by

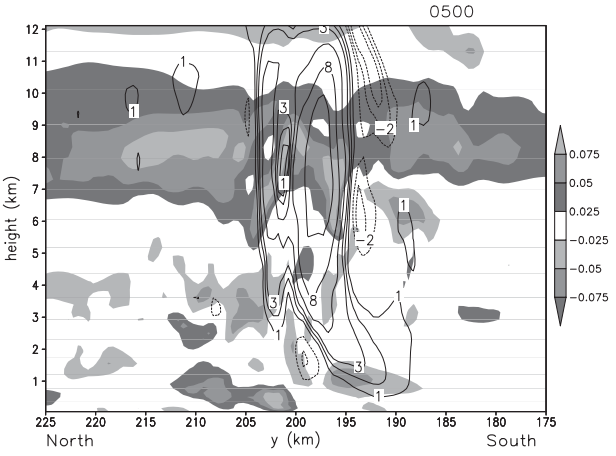

FIG. 9. As in Fig. 8a, but the shaded field is buoyancy (m s^{-2}) and wind vectors have been removed for clarity. The buoyancy field was calculated using Eq. (35) of Bryan and Fritsch (2002) and includes hydrometeor loading effects.

Raymond and Rotunno (1989) and Haertel et al. (2001), and the idea of low-level gravity waves or bores as maintenance mechanisms for mesoscale convective systems has been put forth by Dudhia et al. (1987), CM88, Schmidt and Cotton (1990), and Parker (2008), However, Dudhia et al. (1987), CM88, and Schmidt and Cotton (1990) used two-dimensional simulations, and it is shown here—at least for environments in which quasi-stationary MCSs develop—that three-dimensional effects are important. Unlike Parker's simulation, which transitions from a cold-pool-driven squall line to one with a low-level gravity wave, the gravity wave is the initial structure here. This difference likely comes about because the initial thermodynamic environment here is stable at low levels, whereas Parker (2008) increased the stability over time by adding low-level cooling. SJ08 presented a case study with observations and simulations suggesting the importance of a low-level gravity wave in organizing a flash-flood-producing MCS. Raymond and Rotunno (1989) and Haertel et al. (2001) showed that gravity waves result when cooling (such as that from evaporation) is applied to stable flow, although SJ08 found that the waves in this thermodynamic environment result from latent heating rather than cooling. As such, based on the results of the real data simulation in SJ08 and in the idealized simulation shown here, we can conclude that low-level gravity waves are a fundamental, though often overlooked, mechanism for the organization of linear convective systems, especially in very moist environments that are not supportive of strong cold pools. The dynamics governing the development of these waves and their propagation is a subject of ongoing research.

b. Observational evidence for low-level gravity waves

Considering the relatively coarse resolution of the surface observing network in much of the central United States and the relatively small size of some of the observed MCSs, observations of the low-level gravity waves discussed above are few. However, in one of the events discussed in SJ09, which occurred on 20 August 2007 in Missouri, the convective line passed over two automated surface stations that reported data every minute. At 0745 UTC (Fig. 12a), the MCS is developing over southwest Missouri with a linear band of convection oriented from southwest to northeast. As this convective line passes over the Joplin, Missouri observing station (denoted JLN in Fig. 12a) between approximately 0735–0810 UTC, 1-min surface observations show several undulations in the pressure field, with the wind field generally varying in phase with the pressure (Fig. 12b). This behavior is consistent with that of a gravity wave (e.g., Koch and Golus 1988). Also of note at this time are the large rainfall rates associated with the convective line: 1-min rainfall totals reach 2 mm, which converts to an instantaneous rainfall rate of 120 mm h^{-1} (4.8 in h^{-1}).

Somewhat later, at 0930 UTC, the convective line passes over the Springfield, Missouri observing station (denoted SGF in Fig. 12c). Although the phase relationship between pressure and wind during the convection's passage at this station is not quite as strong as at Joplin, these two fields do vary in phase between approximately 0920 and 0945 UTC during a period of convective rainfall (Fig. 12d). Furthermore, over the time periods shown in Figs. 12b,d, the surface temperature changed by no more than 1°F (0.56°C), with the temperature actually rising by 1°F at Joplin (not shown). The resolution of the available temperature observations is only 1°F, which prevents a more detailed analysis of the temperature field, but the minimal temperature changes suggest that the convection is most likely not being organized and maintained by a surface cold pool/density current. Although the observations shown in Fig. 12 are limited, they provide some evidence for the idea that low-level waves are assisting in the organization of these extreme-rain-producing convective systems. Observations of such MCSs with a denser observing network could provide more substantial information about their surface features.

c. Evolution of convective system at later times

As discussed above, the integration of the 1-km simulation was carried out beyond the 5 h of the 500-m simulation. The convective system at later times exhibits some characteristics that contrast with how it initially became organized (Fig. 5). The gravity wave discussed

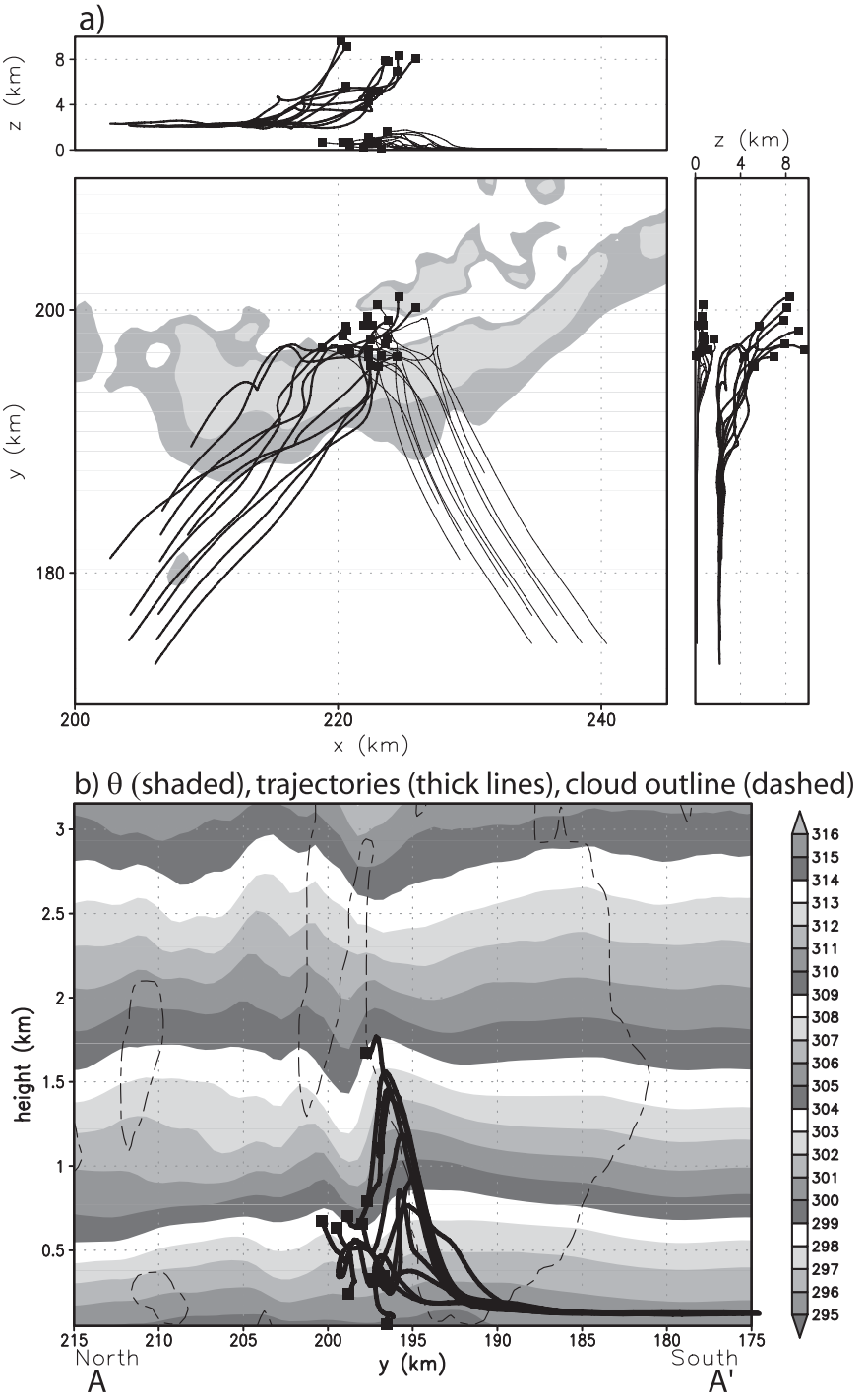

FIG. 10. (a) Projection of selected 3D air parcel trajectories onto Cartesian planes in the 500-m simulation. The trajectories are shown from $t = 4$ h to $t = 5$ h and the end of each trajectory is marked with a square. The thin trajectories originated at approximately 0.125 km above the surface, and the thick trajectories originated at approximately 2.1 km. In the x–y plane diagram, the $\theta' = -0.5$ and -1 K contours at $t = 5$ h are shaded to show the location of the low-level gravity wave. (b) North–south vertical section showing potential temperature (shaded every 1 K), cloud outline (thin dashed line), and the near-surface trajectories from (a) in the lowest 3 km to emphasize the low-level structure. The location of the cross section and the averaging are the same as in Fig. 8a.

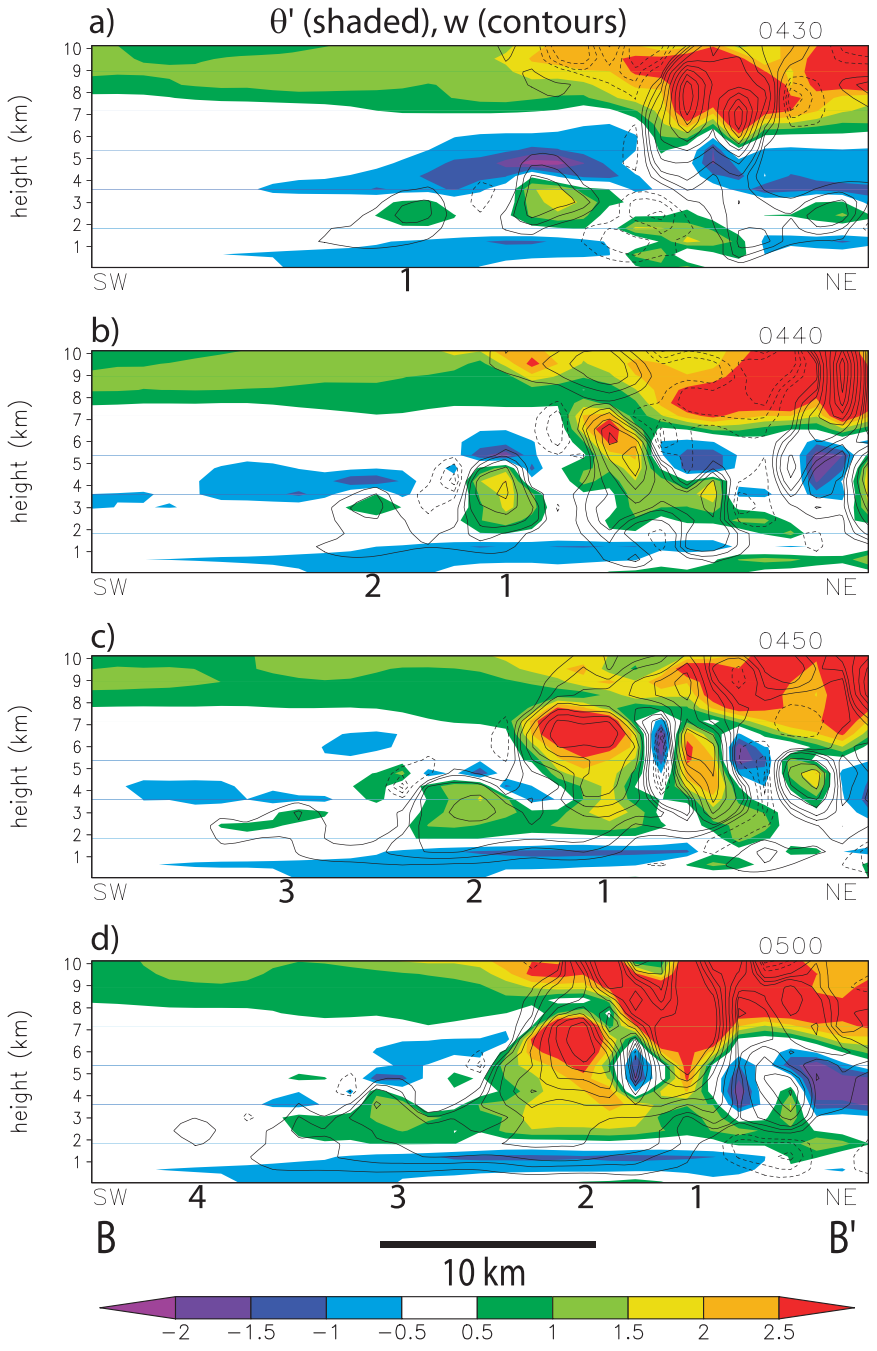

FIG. 11. Series of southwest-to-northeast sections showing the development of several convective cells in the 500-m simulation. The location of the sections is shown by line B–B′ in Fig. 7b. Shown are potential temperature perturbations (K; shaded as shown) and vertical velocity (line contours at ±1, 2, 3, 5, 7, 9, 11, 13, and 15 m s^{-1}, with negative contours dashed). The numbers 1–4 denote specific cells discussed in the text. Times shown are (a) 4.5 (4 h 30 min), (b) 4.67, (c) 4.83, and (d) 5 h.

above was the primary low-level structure through approximately t = 7.5 h, but after this time a cold pool began to develop and quickly altered the convective organization (Fig. 13). At t = 7 h (Fig. 13a), the first signs of a cold pool are appearing, but the deep convective lines are still associated with the low-level gravity wave, which is only barely visible at the surface but is strongest at ~1 km AGL (cf. Fig. 7). By t = 9 h (Fig. 13c), however,

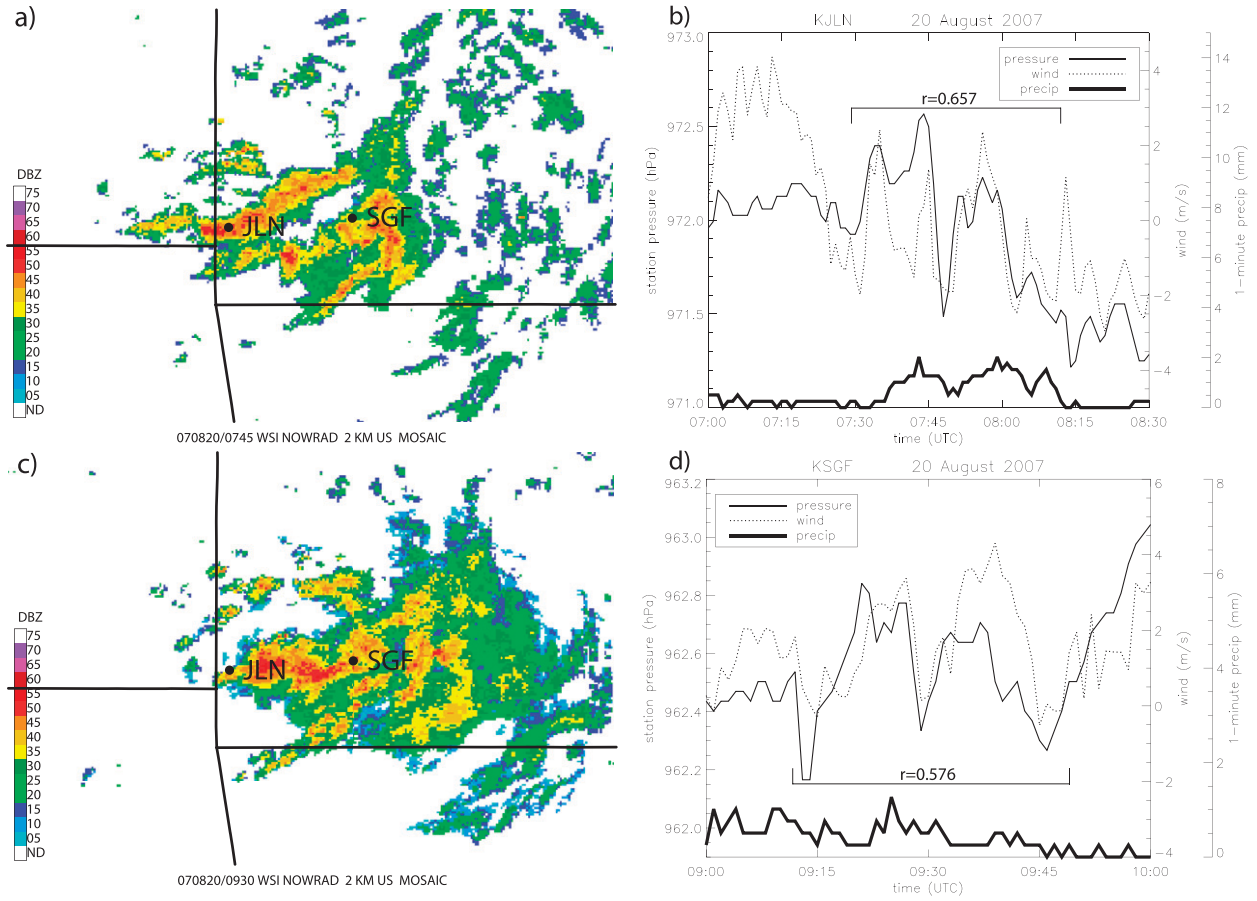

FIG. 12. (a),(c) Observed composite radar reflectivity at (a) 0745 and (c) 0930 UTC 20 Aug 2007. Also shown are the locations of surface observing stations at Joplin (JLN) and Springfield (SGF), Missouri. (b),(d) Time series showing station pressure (hPa; solid line) and wind speed in the direction of wave propagation (m s^{-1}; dotted line) on 20 Aug 2007 for (b) station JLN from 0700 to 0830 UTC and (d) station SGF from 0900 to 1000 UTC. Also shown (thick solid lines) is precipitation accumulated in the previous minute (mm). The winds were calculated using Eq. (1) of Koch and Golus (1988), using 270° as the direction from which the wave was propagating (measured clockwise from north) for the earlier time shown in (a) and (b) and 290° for the later time shown in (c) and (d). Also shown on the surface time series are correlation coefficients between the pressure and wind fields, calculated over the indicated time periods.

the cold pool has become much stronger and has spread toward the south. Deep convection is still occurring at this time, but it has become less organized and does not have the distinctly linear pattern that existed earlier. Additionally, the deep convection is not located at the leading edge of the cold pool; rather, it is displaced 20–30 km behind the gust front. By the end of the simulation (Fig. 13d), the convection has weakened even further, and by this time an extensive region of stratiform rainfall has developed behind the dissipating convective line (Fig. 5e). This evolution is consistent with Parker (2007), who found that MCSs with parallel stratiform precipitation undergo a ''seemingly inexorable march toward [trailing stratiform] structure.''

The vertical cross section in Fig. 14 shows an example of some of the processes involved in the transition between the gravity wave and cold-pool-driven stages of the convective system. At $t = 8$ h (Fig. 14a; a plan view at the same time is shown in Fig. 13b) the low levels still show some signs of the gravity wave, but the near-surface cold pool is also intensifying and is beginning to spread southward. There is a weak updraft at the leading edge of the cold pool (above approximately $y = 227$), but the deep convection is located farther to the north. As the cold pool spreads southward, the convection becomes more tilted and further removed from the cold pool edge. At $t = 8.58$ h, however, a pocket of cold air, along with inflow from the rear of the system, appears and causes the deep convective cells to become upright once again (Fig. 14b). These temperature and wind perturbations, which are located at approximately 3–4.5 km AGL above $y = 245$–250, resemble the elevated rear-inflow jets discussed by Weisman (1992), which he argued could assist in keeping a convective line upright when the horizontal

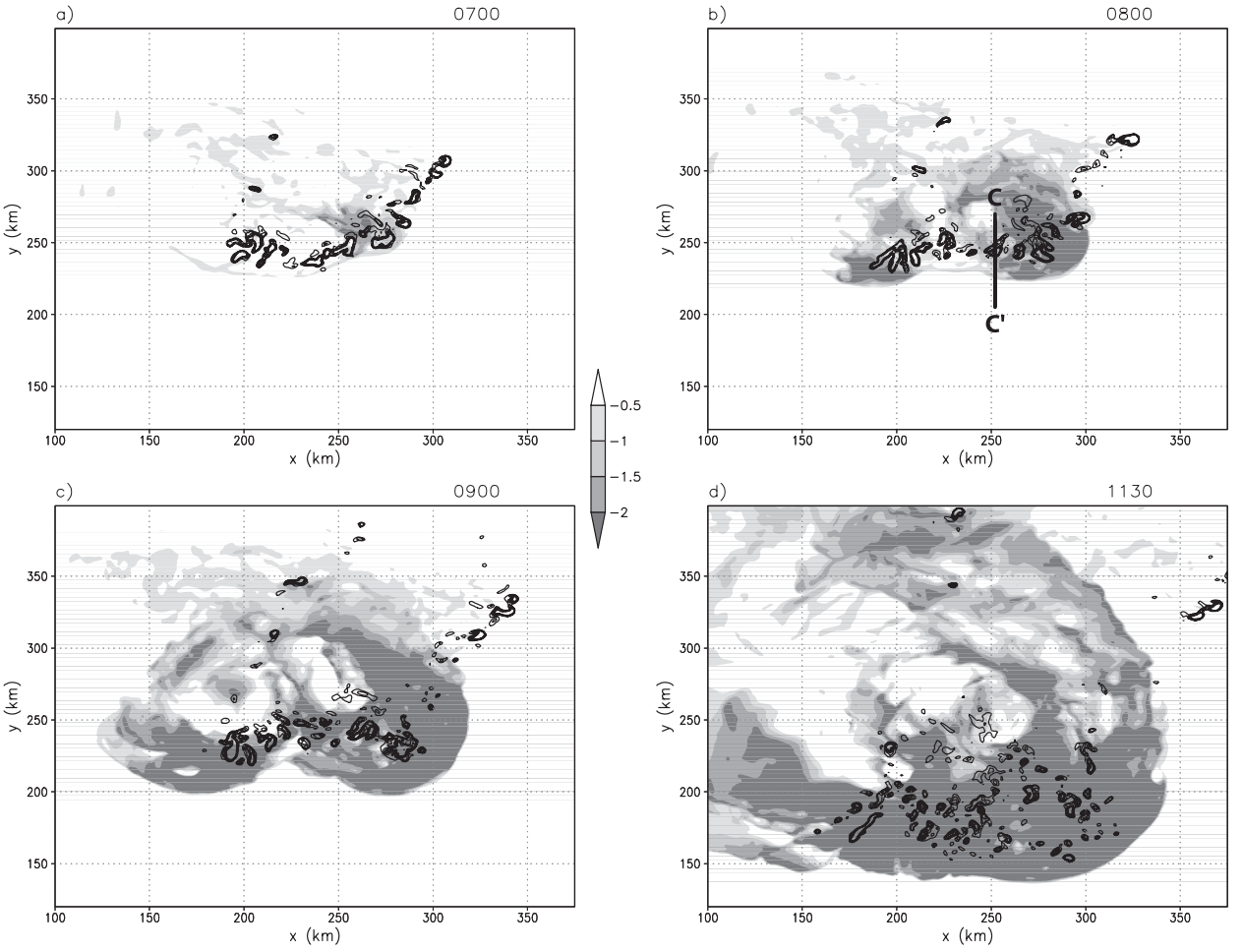

FIG. 13. Potential temperature perturbations (K; shaded) on the lowest model level and vertical velocity at 7 km AGL (contoured every 2 m s^{-1} above 2 m s^{-1}) at t = (a) 7, (b) 8, (c) 9, and (d) 11.5 h of the 1-km simulation. Line C–C′ indicates the location of the vertical cross section to be shown in Fig. 14.

vorticity from the cold pool overwhelms that from the ambient shear. The rear-inflow jet and elevated cool pockets also apparently contribute to the near-stationarity of deep convective activity (above y = 240–245) in the 35-min period shown here, even though the surface cold pool has surged southward substantially to y = 215.

In this simulation, it takes a long time for a cold pool to develop owing to the nearly saturated midlevels, and the cold pool that does develop is very shallow because the subsaturated layer near the surface is also very shallow. Once the cold pool forms, however, it strengthens rapidly, which appears to occur in association with the downward transport of air with low equivalent potential temperature θ_e [Fig. 15, as discussed by, e.g., Rotunno et al. (1988)]. At t = 6.75 h (Fig. 15a), θ_e varies little near the surface beneath the convective line, but the south–north gradient is stronger aloft owing to the presence of the gravity wave at approximately 1 km AGL (above approximately y = 240) as well as lower θ_e air to the north. An hour later (Fig. 15b), a descending rear-inflow jet (e.g., Weisman 1992) has begun to form, and low-θ_e air has descended to the ground. Below 3 km, the updraft is now significantly tilted as the surface cold pool begins to develop. By t = 8.25 h (Fig. 15c), the cold pool has strengthened and is surging southward.

The transition from a gravity-wave-driven to a cold-pool-driven convective line is similar to that in the two-dimensional simulations of CM88 and Lafore and Moncrieff (1989). However, the tendency of the convection to become less organized after the development of a strong cold pool is different from most past studies of convective systems. In this simulation, the cold pool spreads southward in an environment that is suboptimal in terms of the theory of Rotunno et al. (1988) because the horizontal vorticity at the edge of the cold pool is of the same sign as that of the shear in the lowest 1 km. However, the reversal of the shear above the cold pool allows moist, conditionally unstable air to continue to

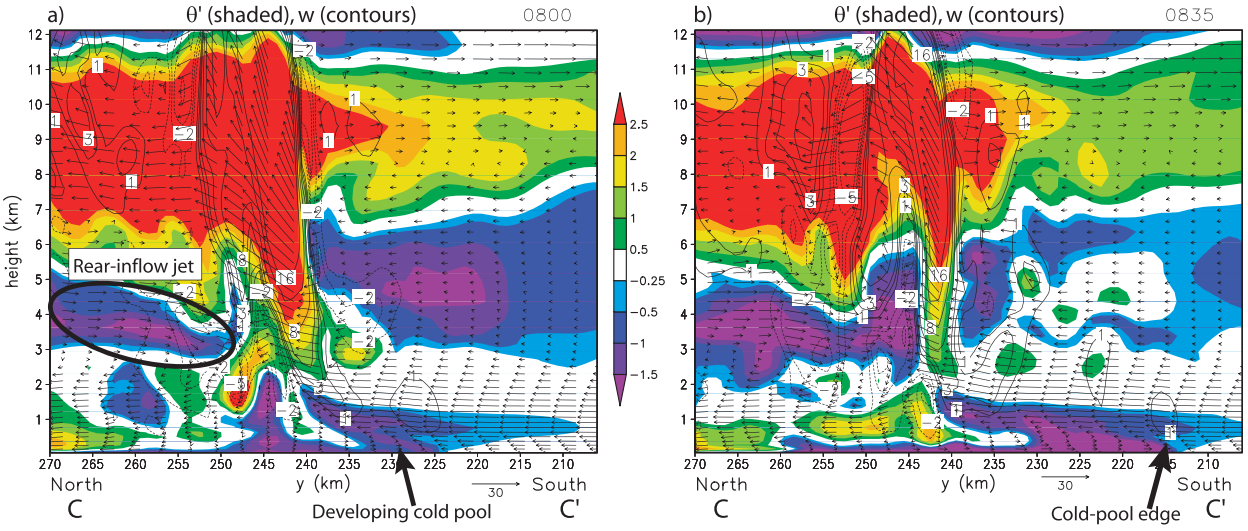

FIG. 14. As in Fig. 8, except for the cross-section location shown by line C–C′ in Fig. 13b at t = (a) 8 and (b) 8.58 h of the 1-km simulation. However unlike Fig. 8, values have not been area averaged.

flow into the system from the south, and the large-scale lifting and rear-inflow jet assist in maintaining some deep convection even though the surface cold pool has undercut the system. This evolution bears at least some similarity to a few of the observed extreme-rain-producing convective systems in SJ09 as well, particularly the 5–6 May and 3–4 June 2000 events. In both of those cases, the primary convective lines remained quasi-stationary for several hours, after which there were southward surges of convection consistent with the spreading of a cold pool. Yet even after these surges took place, other clusters of convection within these MCSs continued to back-build and move slowly.

Although accumulated rainfall is not one of the best-performing output fields for cloud models (Gilmore et al. 2004), the purpose of these simulations is to understand convective systems that produce locally extreme rainfall that has the potential to cause flash flooding. If the simulated rainfall amounts are not consistent with observations, it would be a dubious claim that these were faithful simulations of extreme-rain-producing MCSs. For the purposes of comparing the simulated rainfall with an actual event, the rainfall field (translated to account for the moving domain) has been projected onto a map and is shown next to accumulations from the simulation of the 6–7 May 2000 case presented in SJ08 (Fig. 16).[2] Through 11 h, the accumulated rainfall from the idealized simulation compares favorably with the 6–7 May 2000 case, although the rainfall was more widespread in that event. The maximum rainfall in the idealized simulation through 11 h was 136 mm (5.35 in), whereas it was 172 mm (6.77 in) in the case-study simulation. In the 6–7 May event, the heavy rainfall continued for several hours beyond the time shown here, but in the idealized simulation the heaviest rain has ended by t = 11 h because of the southward movement and weakening of the convective line. A strong cold pool never formed in the 6–7 May 2000 event, which allowed it to continue producing locally heavy rainfall for a longer period of time; this may be partially attributable to additional moisture transport by the LLJ in the real case. In the region of maximum rainfall amounts in the idealized simulations, most of the rain fell in about a 4-h period (t = 5–9 h). Given these local rainfall totals in excess of 25 mm h^{-1} for several hours and the accurate representation of the back-building, quasi-stationary characteristics of observed systems, and considering the uncertainties in model-predicted rainfall, it appears that this is generally a faithful idealized simulation of an extreme-rain-producing MCS.

4. Sensitivity experiments

Several numerical experiments were carried out to test the sensitivity of the simulated convective systems to various processes. These sensitivity experiments are summarized in Table 2. Other than the changes listed in Table 2 and discussed in this paragraph, these simulations are identical to the 1-km simulation presented

[2] Data from the SJ08 simulation is used here instead of rain gauge observations so that a particular 11-h period can be compared. SJ08 showed that it was a reasonably accurate simulation of the 6–7 May 2000 case, and selecting particular hours was not possible with the relatively sparse hourly rain gauge network.

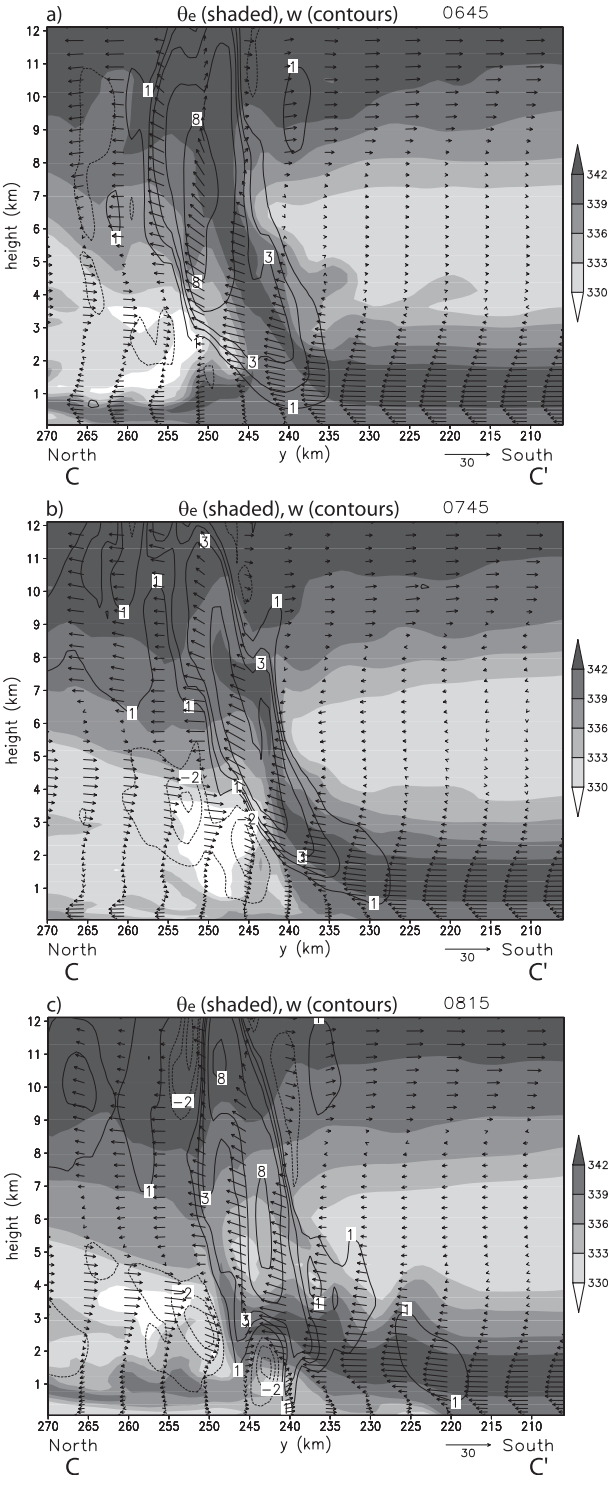

FIG. 15. North–south vertical cross section, located along line C–C′ in Fig. 13b, showing equivalent potential temperature (K; shaded), vertical velocity (contoured as in Fig. 8), and system-relative, line-perpendicular flow vectors (m s^{-1}). Values have been averaged over an area 5 km on either side of the line.

above, which will be referred to as CTRL in the discussion to follow. For the microphysical sensitivities (NOEVAP and NOMELT), the code of the microphysics scheme was modified so that phase changes occur as usual, but no latent cooling occurs when the respective phase changes take place. In NOEVAP, the cooling is only removed for the evaporation of rainwater; evaporation of cloud water is unchanged. In STOPFORCE, the momentum forcing is applied for the first 2 h of the simulation and is then removed. This provides the lifting necessary to initiate convection initially and then tests whether deep convection can be maintained without additional forcing. After the forcing is removed, the associated convergence and vertical motion weaken quickly, but some lifting does remain (Fig. 17). The CORIOLIS experiment was designed to test the effects of planetary rotation on the simulated convection. In this run, the Coriolis force is only applied to perturbations from the base-state wind. However, this means that Coriolis accelerations are also acting on the imposed forcing, the physical meaning of which is not entirely clear because the forcing is applied artificially. Nonetheless, a dry simulation shows that the resulting flow fields in CORIOLIS are broadly similar to that in CTRL, although the upward motion owing to the forcing is slightly weaker (Fig. 18; cf. Fig. 3b) and the stronger wind perturbations have experienced a noticeable deflection due to Coriolis accelerations. As such, CORIOLIS and CTRL are not exactly comparable because the imposed forcing is not identical between the two runs. However, the primary effects of planetary rotation can still be examined. In this run, the value of the Coriolis parameter, which is constant across the domain (i.e., an *f* plane), was chosen to correspond to the latitude of Springfield, Missouri (37.25°N). Finally, a run in which the height of the convergence maximum is changed, referred to as LOWFORCE, is discussed briefly in section 4d.

a. Microphysical processes

The first two sensitivity experiments were designed to test the importance of specific microphysical processes on the simulated convection. CM88 removed evaporation of rain in their simulations and found that in an environment with large-scale lifting, a cold pool (produced by evaporative cooling) was not necessary for maintaining a squall line. Because the convective system discussed in section 3 initially became organized despite the lack of a cold pool, a similar simulation is employed here to understand the role of latent cooling in organizing and maintaining the convection.

Somewhat counterintuitively, the simulation without cooling from evaporation of rainwater (NOEVAP) has

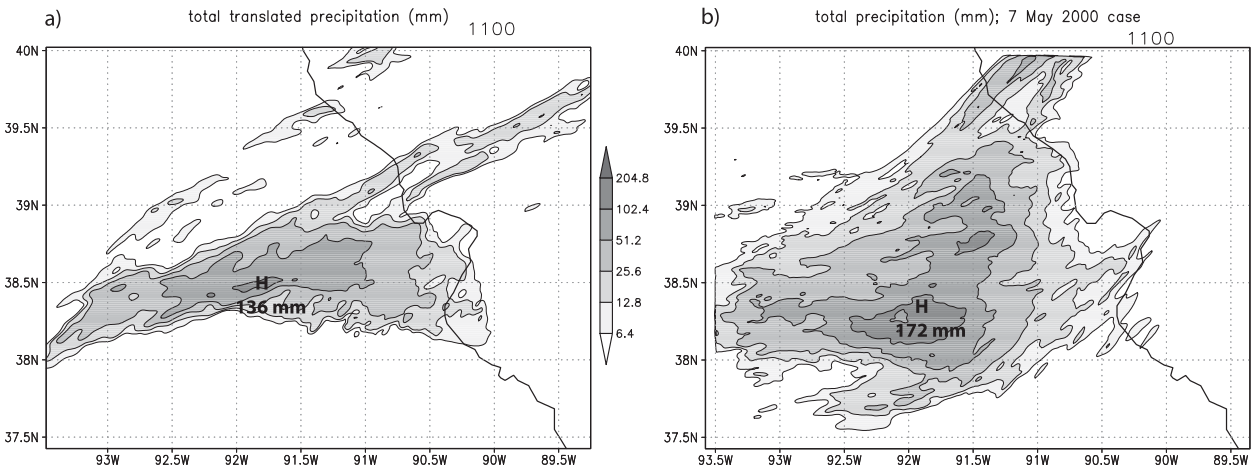

FIG. 16. Comparison of accumulated rainfall between the idealized simulation and a realistic simulation of an actual event. (a) Accumulated rainfall through $t = 11$ h in the 1-km idealized simulation. (b) Accumulated rainfall from 0000–1100 UTC 7 May 2000, from the simulation presented in SJ08. The rainfall data in (a) have been translated to remove the effects of the moving model domain, and they have been projected onto the same map that is shown in (b) for purposes of visual comparison.

consistently stronger convection than the control run or any of the other sensitivity tests (Fig. 19). Through the first 4 h of NOEVAP, the convection initiates and evolves similarly to CTRL (not shown). There are indications of linear organization and back-building along the same low-level gravity waves discussed previously. However, in the later stages of NOEVAP, two clusters of convection separate from each other: most of the convection moves quickly toward the northeast, while a smaller cluster remains near the center of the domain within the convergence region (Figs. 20b and 21b). By $t = 9$ h, a loosely organized line of intense convective cells was located in the northeast part of the domain (Fig. 21b), signifying that the most intense convection had actually moved away from the forcing. Furthermore, it propagated in this direction without any contribution from a density current; the maximum surface potential temperature deficit is less than 1 K.

The convective system in NOMELT is organized more like CTRL than NOEVAP. It has a back-building southwest–northeast-oriented convective line in a similar location (Figs. 20c and 21c). Although the maximum vertical velocities in NOMELT are comparable to those in CTRL (Fig. 19), the distribution of deep convection differs. In NOMELT, there are just a few intense convective cores, which are mainly located near the momentum forcing. However, there is a large region of weaker, less organized convection throughout much of the domain, in contrast with the more focused line in CTRL. Also, a surface cold pool never forms in the 9 h of integration of NOMELT, suggesting that melting effects were very important in the development of the cold pool that formed in the later stages of CTRL, as discussed by Atlas et al. (1969) and others.

The differing organization and motion of the convection in NOEVAP compared with CTRL and NOMELT suggests that the evaporation of rainwater can have important effects on convection in addition to cold-pool development. Although it was shown previously that a latent-heating-related gravity wave, rather than a cold pool, was the organizing mechanism in the first several hours of the simulations, evaporative cooling apparently still plays an important role in keeping the convective system quasi-stationary. Or in other words, evaporative cooling is not necessary to maintain a vigorous convective system, but it does affect its organization. In both CTRL and NOMELT (Figs. 21a,c), the convection was organized from southwest to northeast and exhibited significant back-building behavior. In NOEVAP (Fig. 21b), on the other hand, the convection

TABLE 2. Descriptions of the sensitivity experiments. Additional details are given in the text.

CTRL	Primary 1-km simulation discussed in section 3
NOEVAP	No latent cooling from evaporation of raindrops
NOMELT	No latent cooling from melting or sublimation of graupel and snow
STOPFORCE	Momentum forcing is removed after 2 h
CORIOLIS	Coriolis force included, with $f = 8.882 \times 10^{-5}$ s^{-1}
LOWFORCE	Vertical center point of imposed convergence lowered to 1 km AGL

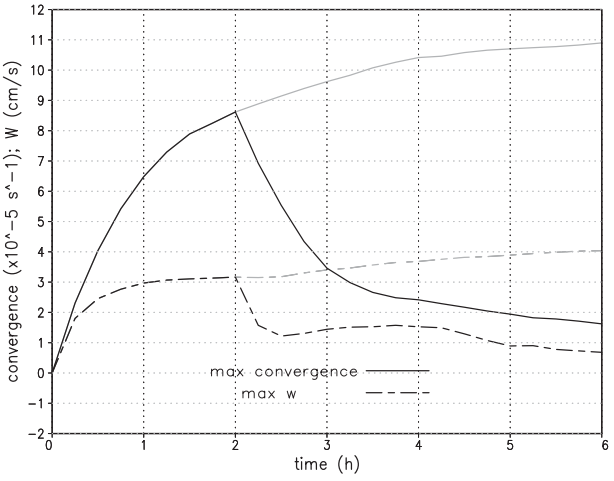

FIG. 17. As in Fig. 3a, but for STOPFORCE (in a dry simulation), where the momentum forcing is turned off after 2 h of integration. The time series for CTRL are shown in gray for comparison.

raced toward the northeast and was organized very differently. Thus, processes resulting from evaporative cooling are evidently responsible for pushing the convective line southward, although it is not entirely clear how these processes come about when the potential temperature has only been cooled by a fraction of a degree and the buoyancy field has not been substantially altered by hydrometeor loading (Fig. 9).

b. *STOPFORCE*

Experiment STOPFORCE identifies the role of the imposed forcing and tests whether a strong convective system can be maintained even after this forcing has been removed. Of particular interest in designing this simulation is the finding of CM88 that "if the environmental air is lifted to its level of saturation over a wide region before the initiation of convection, then the lifting at the cold pool is no longer critical in maintaining the convective system." Simulation STOPFORCE tests this assertion in a more sophisticated model.

Although the convective system that develops in STOPFORCE is not quite as strong as that in CTRL, it is nonetheless organized very similarly and shows no signs of weakening through 9 h of integration (Figs. 20d and 21d). Furthermore, the convective line is organized linearly and maintained without forcing or a cold pool through most of the simulation; only after approximately 8 h does a surface cold pool begin to appear (Fig. 19). The low-level mechanism responsible for organizing the system through $t = 8$ h of STOPFORCE is the same low-level gravity wave discussed previously (not shown).

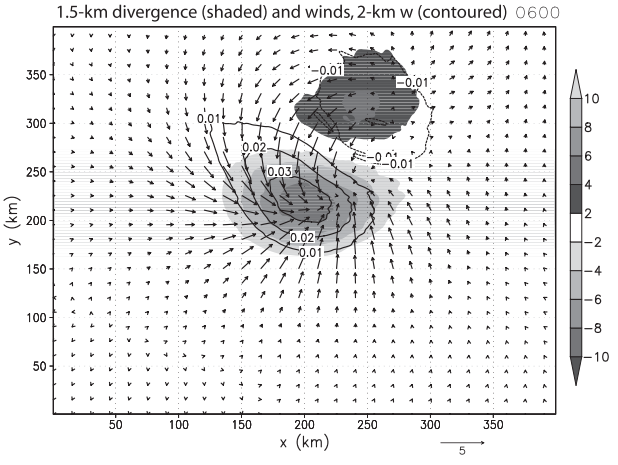

FIG. 18. As in Fig. 3b, but for CORIOLIS (in a dry simulation).

The short-distance mechanism for back-building along the low-level wave illustrated in Fig. 11 is also at work in this simulation. This demonstrates that even though the background convergence can lift parcels to their LFC (and it does so to initiate the very first convective cells), once a large region of saturation has been attained and deep convection has been initiated, in this shear profile the convection will organize into a back-building line on its own.

c. *CORIOLIS*

Experiment CORIOLIS considers the effect of planetary rotation on the simulated convective systems. Because the Rossby radius of deformation decreases with increasing latitude (e.g., Holton 2004), the distance that gravity waves can propagate away from their source

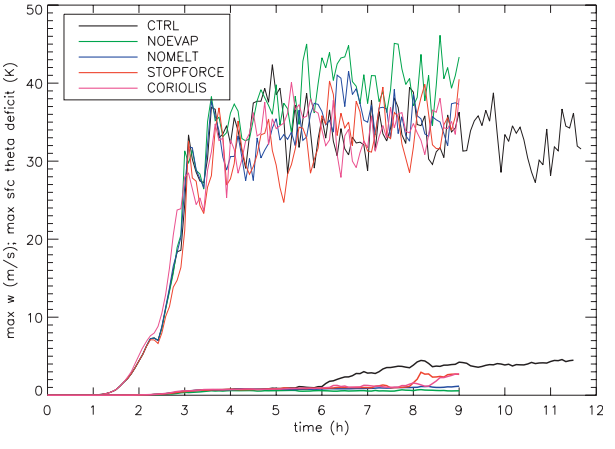

FIG. 19. Time series comparing the sensitivity simulations. The traces at top show the maximum vertical velocity (m s^{-1}), and those at the bottom show the maximum θ deficit (K) on the lowest model level. Recall that the control run was integrated for 11.5 h, whereas the other runs were only integrated for 9 h.

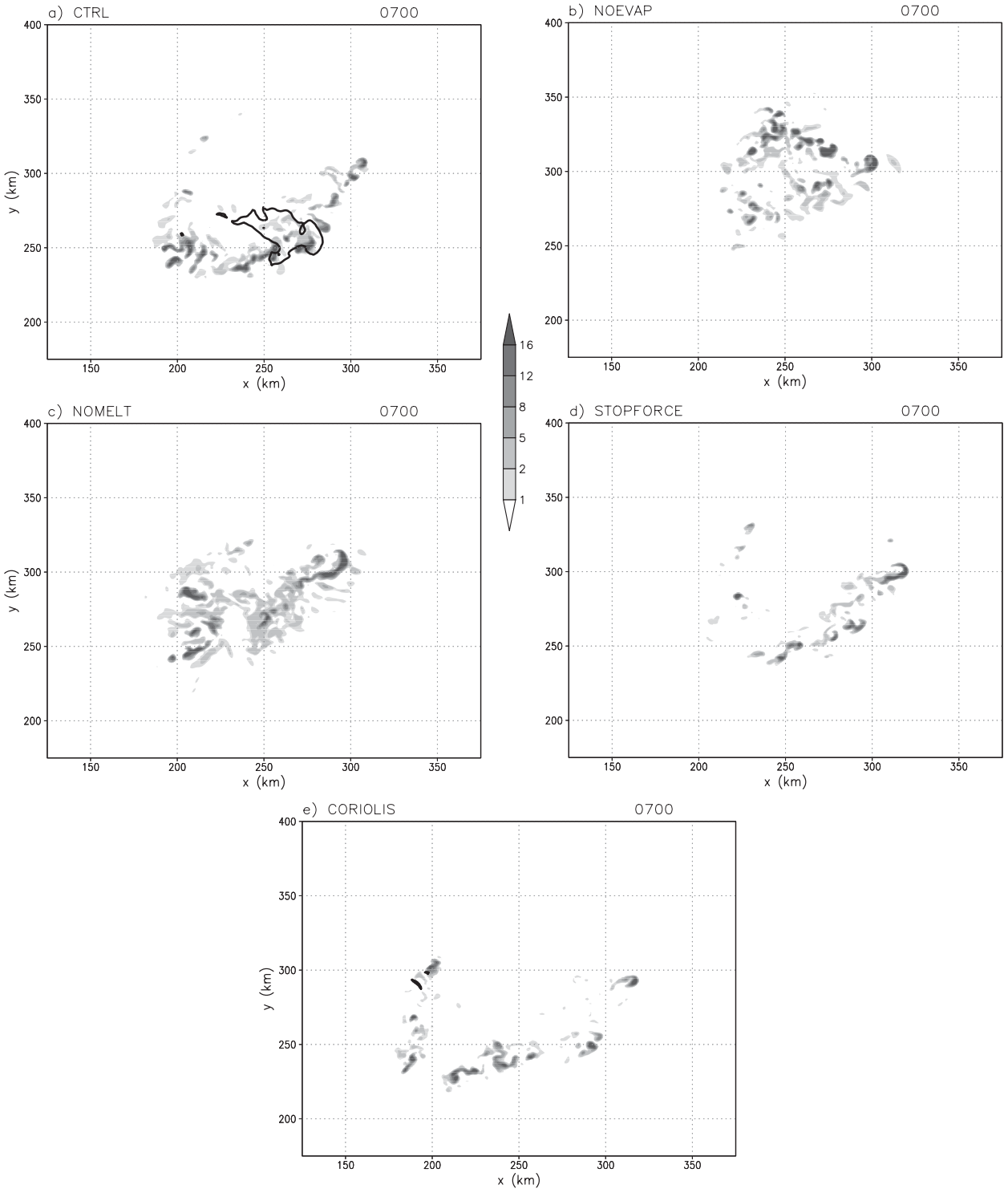

FIG. 20. Vertical velocity (m s^{-1}) at 7 km AGL for (a) CTRL, (b) NOEVAP, (c) NOMELT, (d) STOPFORCE, and (e) CORIOLIS at $t = 7$ h. Also shown by a thick black line, where applicable, is the $\theta = -1$ K contour on the lowest model level to denote the cold pool outline. The same portion of the model domain is shown in all panels, and the background convergence is centered at $x = y = 200$ km, with the domain translating as discussed in the text.

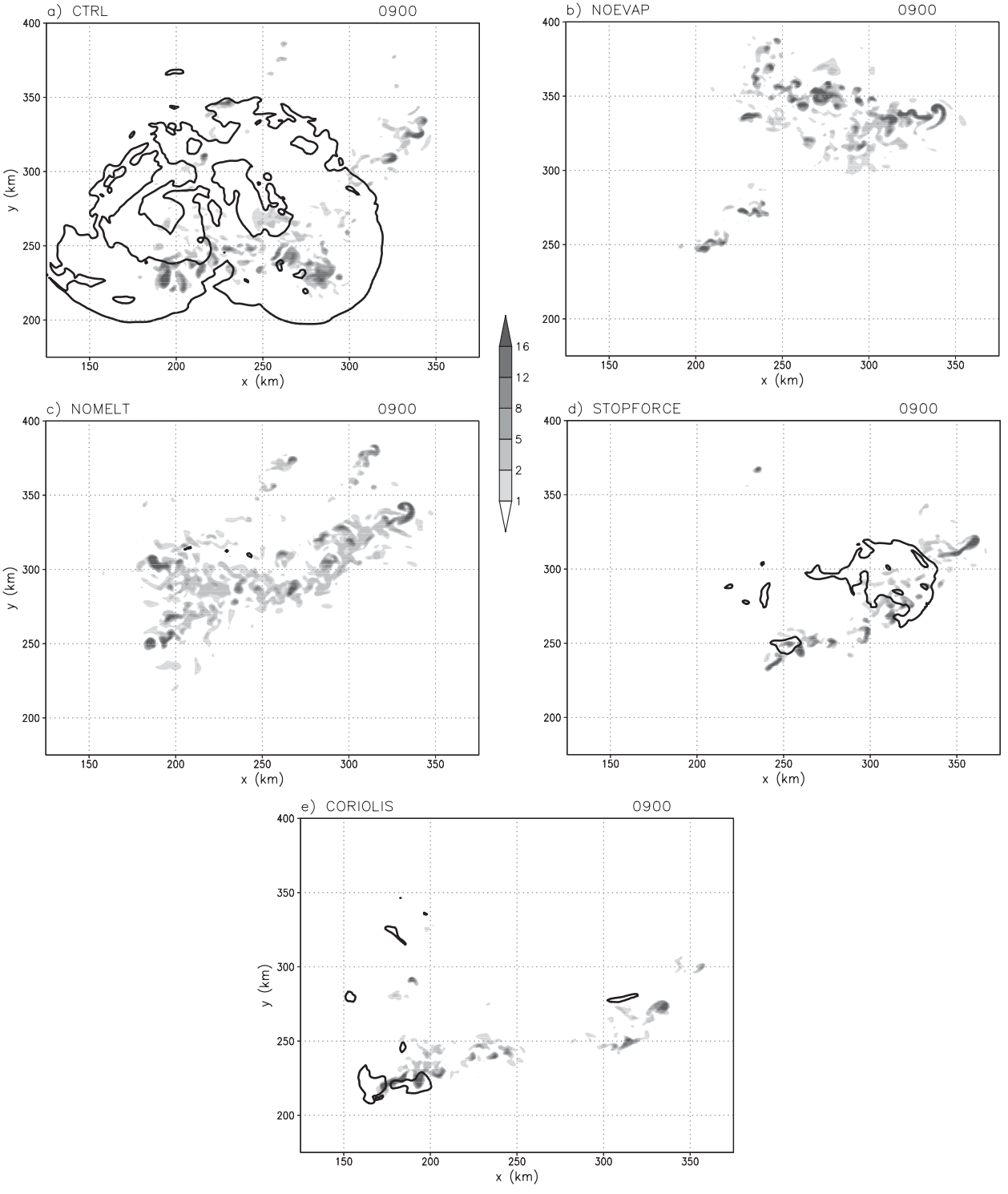

FIG. 21. As in Fig. 20, but at $t = 9$ h.

is shorter in the midlatitudes than in the tropics. Mapes (1993) and Liu and Moncrieff (2004) found that adiabatic displacements associated with convectively generated gravity waves can make the nearby environment more favorable for convection and that the ability for waves to propagate longer distances at lower latitudes makes clustering of convection more prominent there. Planetary rotation can have other effects on midlatitude

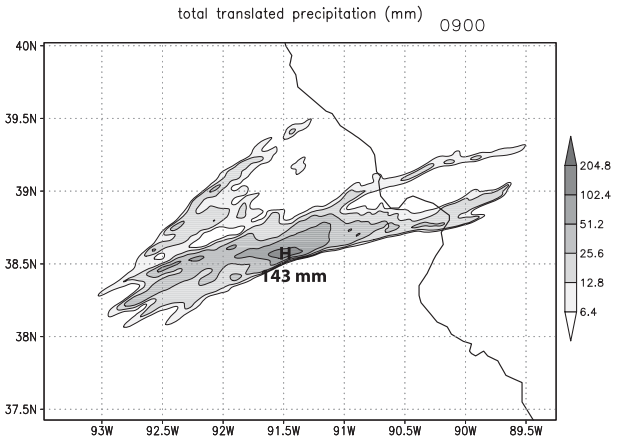

FIG. 22. As in Fig. 16, but for CORIOLIS through $t = 9$ h.

convection, such as favoring the evolution of squall lines toward an asymmetric structure and altering the characteristics of MCVs (e.g., Skamarock et al. 1994; Davis and Weisman 1994). Because the observed MCSs of interest are midlatitude phenomena, it is important to test whether the previously presented simulations, which had $f = 0$, are still representative of the observed system when f is nonzero. Through the first 5 h of CORIOLIS, convection initiates and evolves almost identically to the CTRL run (Fig. 19). After $t = 5$ h, the convection in CORIOLIS does not organize and strengthen quite as quickly as in CTRL, but it still organizes into a southwest-to-northeast back-building line by $t = 7$ h. The length of the line is similar to that in CTRL, but it is not as intense (Fig. 20e). Again, the low-level organizing mechanism is a gravity wave (not shown). The simulations diverge after $t = 7$ h: a cold pool develops and dominates the evolution of the system in CTRL, whereas in CORIOLIS a cold pool fails to develop and the length of the convective line decreases. By $t = 9$ h, the line in CORIOLIS is much smaller than that in CTRL (Fig. 21e), but it is still quite intense. It has also moved toward the southwest relative to the forcing, and this led to a very long period of ''echo training.'' In fact, the maximum point rainfall total through 9 h in CORIOLIS is larger than that through 11 h in CTRL, even though the convective system is smaller in size (Fig. 22; cf. Fig 16a). A small MCV (with diameter of about 50 km) does form near the end of the simulation (at approximately $t = 8$ h); it is similar to those described by Davis and Weisman (1994) but does not appear to have a strong effect on the evolution of the system in the last hour of the run. Determining the reasons for the strong propagation toward the southwest in CORIOLIS is beyond the scope of this study and warrants further investigation.

d. LOWFORCE

The final sensitivity experiment, LOWFORCE, was motivated by the comment of an anonymous reviewer of the original manuscript. This reviewer questioned whether the downward motion (and related downward-pointed pressure gradient force) near the surface (as shown in Fig. 3) was a realistic representation of forcing by an MCV, which could have an upward-directed pressure gradient force everywhere owing to the vortex's low pressure center at midlevels. Although the method used in this study for imposing elevated convergence will necessarily have descent somewhere below the convergence maximum (which may be unrepresentative of real MCVs), one way of testing the sensitivity to the shallow low-level descent is by moving the convergence maximum somewhat closer to the model surface. LOWFORCE places the maximum convergence at 1 km AGL (as opposed to 1.5 km AGL in CTRL), and the resulting divergence profile is shown in Fig. 23a. In fact, the simulated convective system that develops in LOWFORCE organizes more quickly, remains quasi-stationary for somewhat longer, and produces a larger accumulated rainfall maximum than CTRL (Fig. 23b); thus, it is perhaps an even better simulation of a quasi-stationary MCS than CTRL. The processes that were important in CTRL (such as the role of the gravity wave and the lack of a cold pool) were also important in LOWFORCE, so the conclusions presented earlier are unchanged.

5. Conclusions

In this study, idealized simulations of quasi-stationary convective systems, which were designed to understand the workings of convection that forms and organizes within an environment of mesoscale to synoptic-scale lifting, such as is provided by an MCV or other midlevel circulation, were presented. The thermodynamic profile, which was a composite from several extreme rainfall events, was nearly saturated at midlevels, and the wind profile included a strong reversal of wind shear with height associated with a low-level jet. To initiate convection, a momentum forcing was applied, which created elevated convergence that lifted layers of air to saturation and initiated deep moist convection after a few hours. This forcing allows for a realistic examination of convective systems that develop near midlevel vortices without the additional complications of the vortices themselves.

The primary conclusions of this study are as follows:

- Within 2–3 h of initiation, the convection organizes into a back-building line that has similar characteristics

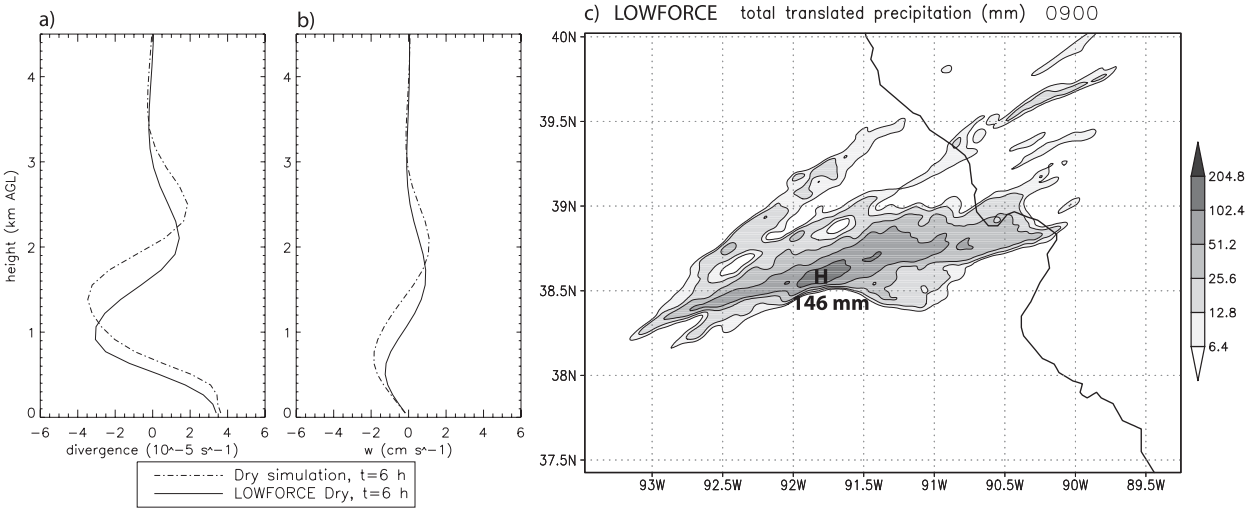

FIG. 23. (a) Vertical profile of divergence, averaged over a 150 km × 150 km box centered on the maximum convergence, for a dry version of LOWFORCE (thick line). The profile from CTRL (also shown earlier in Fig. 3d) is shown in the dashed line for comparison. (b) As in (a), but for vertical velocity. (c) As in Fig. 16, but for LOWFORCE through $t = 9$ h.

to observed extreme-rain-producing convective systems. New convection forms on the southwest end of the line and moves northeast along the line, which leads to large rainfall accumulations at points along the line.

- The initial low-level mechanism for organizing the convective line is not a cold pool but rather a latent-heating-forced gravity wave with a maximum amplitude at approximately 1 km above the surface. Near-surface air rises over this wave and sinks on the other side, but more unstable air above the surface is lifted over the wave, attains its level of free convection, and erupts into deep updrafts. Although this wave may not be necessary for maintaining a vigorous convective system; it clearly helps to determine where and when new cells develop, which affects the organization and the potential for local heavy rainfall production.
- In the later stages of the simulated convective system, a surface cold pool does form. However, it tends to cause the convective line to be less organized, and the continuing deep convection is far separated from the leading edge of the cold pool.
- When the background forcing is removed after convection initiation, the resulting convective system is still strong, long-lived, and quasi-stationary. This suggests that the organization, motion, and maintenance of the system is primarily controlled by the interaction between the shear, the convective heating, and the development of the low-level gravity wave, rather than by the shape and strength of the imposed convergence field.

Although an imposed momentum forcing has been used here, there are almost certainly other justifiable methods for simulating convection that occurs within an environment of large-scale lifting. However, the method used here succeeded in producing physically realistic simulations of quasi-stationary convective systems. Furthermore, the generality of the method used here (and originally developed by CM88 and LWD08) means that it is not limited to the application of midlevel circulations. With appropriate adjustments, it could be used to simulate other situations in which large-scale convergence and lifting occur.

Acknowledgments. The author would like to thank Richard Johnson of CSU for guidance and discussions during the course of this work; George Bryan of the National Center for Atmospheric Research for making his numerical model available and for many helpful insights and suggestions; Adrian Loftus of CSU for discussions regarding convection within mesoscale convergence; Matthew Parker of North Carolina State University for conversations about convective systems and for providing the code to create Fig. 10; Patrick Haertel of CSU for helpful suggestions; and Morris Weisman, Robert Fovell, and an anonymous referee for thorough reviews and suggestions that helped to significantly improve the manuscript. Computing resources were provided by the National Center for Atmospheric Research, which is sponsored by the National Science Foundation. Surface observations used in the creation of Fig. 12 were provided by the National Climatic Data Center. This research was supported by National Science Foundation Grant ATM-0500061.

REFERENCES

Ashley, W. S., T. L. Mote, P. G. Dixon, S. L. Trotter, E. J. Powell, J. D. Durkee, and A. J. Grundstein, 2003: Distribution of mesoscale convective complex rainfall in the United States. *Mon. Wea. Rev.,* **131,** 3003–3017.

Atlas, D., R. Tatehira, R. C. Srivastava, W. Marker, and R. E. Carbone, 1969: Precipitation-induced mesoscale wind perturbations in the melting layer. *Quart. J. Roy. Meteor. Soc.,* **95,** 544–560.

Benjamin, S. G., and Coauthors, 2004: An hourly assimilation-forecast cycle: The RUC. *Mon. Wea. Rev.,* **132,** 495–518.

Braun, S. A., and W.-K. Tao, 2000: Sensitivity of high-resolution simulations of Hurricane Bob (1991) to planetary boundary layer parameterizations. *Mon. Wea. Rev.,* **128,** 3941–3961.

Bryan, G. H., and J. M. Fritsch, 2000: Moist absolute instability: The sixth static stability state. *Bull. Amer. Meteor. Soc.,* **81,** 1207–1230.

——, and ——, 2002: A benchmark simulation for moist nonhydrostatic numerical models. *Mon. Wea. Rev.,* **130,** 2917–2928.

——, J. C. Wyngaard, and J. M. Fritsch, 2003: Resolution requirements for the simulation of deep moist convection. *Mon. Wea. Rev.,* **131,** 2394–2416.

——, R. Rotunno, and J. M. Fritsch, 2007: Roll circulations in the convective region of a simulated squall line. *J. Atmos. Sci.,* **64,** 1249–1266.

Chappell, C. F., 1986: Quasi-stationary convective events. *Mesoscale Meteorology and Forecasting*, P. S. Ray, Ed., Amer. Meteor. Soc., 289–309.

Crook, N. A., and M. W. Moncrieff, 1988: The effect of large-scale convergence on the generation and maintenance of deep moist convection. *J. Atmos. Sci.,* **45,** 3606–3624.

Davis, C. A., and M. L. Weisman, 1994: Balanced dynamics of mesoscale vortices produced in simulated convective systems. *J. Atmos. Sci.,* **51,** 2005–2030.

——, and S. B. Trier, 2007: Mesoscale convective vortices observed during BAMEX. Part I: Kinematic and thermodynamic structure. *Mon. Wea. Rev.,* **135,** 2029–2049.

Doswell, C. A., III, H. E. Brooks, and R. A. Maddox, 1996: Flash flood forecasting: An ingredients-based methodology. *Wea. Forecasting,* **11,** 560–581.

Dudhia, J., and M. W. Moncrieff, 1987: A numerical simulation of quasi-stationary tropical convective bands. *Quart. J. Roy. Meteor. Soc.,* **113,** 929–967.

——, ——, and D. W. K. So, 1987: The two-dimensional dynamics of West African squall lines. *Quart. J. Roy. Meteor. Soc.,* **113,** 121–146.

Durran, D. R., and J. B. Klemp, 1983: A compressible model for the simulation of moist mountain waves. *Mon. Wea. Rev.,* **111,** 2341–2361.

Fovell, R. G., 2002: Upstream influence of numerically simulated squall line storms. *Quart. J. Roy. Meteor. Soc.,* **128,** 893–912.

——, and P.-H. Tan, 1998: The temporal behavior of numerically simulated multicell-type storms. Part II: The convective cell life cycle and cell regeneration. *Mon. Wea. Rev.,* **126,** 551–577.

Fritsch, J. M., R. J. Kane, and C. R. Chelius, 1986: The contribution of mesoscale convective weather systems to the warm-season precipitation in the United States. *J. Appl. Meteor.,* **25,** 1333–1345.

——, J. D. Murphy, and J. S. Kain, 1994: Warm core vortex amplification over land. *J. Atmos. Sci.,* **51,** 1780–1807.

Gilmore, M. S., J. M. Straka, and E. N. Rasmussen, 2004: Precipitation uncertainty due to variations in precipitation particle parameters within a simple microphysics scheme. *Mon. Wea. Rev.,* **132,** 2610–2627.

Haertel, P. T., R. H. Johnson, and S. N. Tulich, 2001: Some simple simulations of thunderstorm outflows. *J. Atmos. Sci.,* **58,** 504–516.

Holton, J. R., 2004: *An Introduction to Dynamic Meteorology*. 4th ed. Academic Press, 535 pp.

Houze, R. A., Jr., 2004: Mesoscale convective systems. *Rev. Geophys.,* **42,** RG4003, doi:10.1029/2004RG000150.

——, S. A. Rutledge, M. I. Biggerstaff, and B. F. Smull, 1989: Interpretation of Doppler weather radar displays of midlatitude mesoscale convective systems. *Bull. Amer. Meteor. Soc.,* **70,** 608–619.

Knievel, J. C., G. H. Bryan, and J. P. Hacker, 2007: Explicit numerical diffusion in the WRF model. *Mon. Wea. Rev.,* **135,** 3803–3824.

Koch, S. E., and R. E. Golus, 1988: A mesoscale gravity wave event observed during CCOPE. Part I: Multiscale statistical analysis of wave characteristics. *Mon. Wea. Rev.,* **116,** 2527–2544.

Lafore, J.-P., and M. W. Moncrieff, 1989: A numerical investigation of the organization and interaction of the convective and stratiform regions of tropical squall lines. *J. Atmos. Sci.,* **46,** 521–544.

Lin, Y.-L., R. D. Farley, and H. D. Orville, 1983: Bulk parameterization of the snow field in a cloud model. *J. Climate Appl. Meteor.,* **22,** 1065–1092.

Liu, C., and M. W. Moncrieff, 2004: Effects of convectively generated gravity waves and rotation on the organization of convection. *J. Atmos. Sci.,* **61,** 2218–2227.

Loftus, A. M., D. B. Weber, and C. A. Doswell III, 2008: Parameterized mesoscale forcing mechanisms for initiating numerically simulated isolated multicellular convection. *Mon. Wea. Rev.,* **136,** 2408–2421.

Maddox, R. A., C. F. Chappell, and L. R. Hoxit, 1979: Synoptic and meso-α scale aspects of flash flood events. *Bull. Amer. Meteor. Soc.,* **60,** 115–123.

Mapes, B. E., 1993: Gregarious tropical convection. *J. Atmos. Sci.,* **50,** 2026–2037.

Miller, M. J., 1978: The Hampstead storm: A numerical simulation of a quasi-stationary cumulonimbus system. *Quart. J. Roy. Meteor. Soc.,* **104,** 413–427.

Nicholls, M. E., R. A. Pielke, and W. R. Cotton, 1991: Thermally forced gravity waves in an atmosphere at rest. *J. Atmos. Sci.,* **48,** 1869–1884.

Parker, M. D., 2007: Simulated convective lines with parallel stratiform precipitation. Part II: Governing dynamics and associated sensitivities. *J. Atmos. Sci.,* **64,** 289–313.

——, 2008: Response of simulated squall lines to low-level cooling. *J. Atmos. Sci.,* **65,** 1323–1341.

——, and R. H. Johnson, 2004: Structures and dynamics of quasi-2D mesoscale convective systems. *J. Atmos. Sci.,* **61,** 545–567.

Raymond, D. J., and R. Rotunno, 1989: Response of a stably stratified flow to cooling. *J. Atmos. Sci.,* **46,** 2830–2837.

——, and H. Jiang, 1990: A theory for long-lived mesoscale convective systems. *J. Atmos. Sci.,* **47,** 3067–3077.

Rotunno, R., J. B. Klemp, and M. L. Weisman, 1988: A theory for strong, long-lived squall lines. *J. Atmos. Sci.,* **45,** 463–485.

Schmidt, J. M., and W. R. Cotton, 1990: Interactions between upper and lower tropospheric gravity waves on squall line structure and maintenance. *J. Atmos. Sci.,* **47,** 1205–1222.

Schumacher, R. S., 2008: Quasi-stationary, extreme-rain-producing convective systems associated with midlevel cyclonic circulations. Ph.D. thesis, Colorado State University, 165 pp. [Available from the Department of Atmospheric Science, Colorado State University, Fort Collins, CO 80523–1371.]

——, and R. H. Johnson, 2005: Organization and environmental properties of extreme-rain-producing mesoscale convective systems. *Mon. Wea. Rev.,* **133,** 961–976.

——, and ——, 2008: Mesoscale processes contributing to extreme rainfall in a midlatitude warm-season flash flood. *Mon. Wea. Rev.,* **136,** 3964–3986.

——, and ——, 2009: Quasi-stationary, extreme-rain-producing convective systems associated with midlevel cyclonic circulations. *Wea. Forecasting,* **24,** 555–574.

Skamarock, W. C., M. L. Weisman, and J. B. Klemp, 1994: Three-dimensional evolution of simulated long-lived squall lines. *J. Atmos. Sci.,* **51,** 2563–2584.

Thorpe, A. J., M. J. Miller, and M. W. Moncrieff, 1982: Two-dimensional convection in non-constant shear: A model of midlatitude squall lines. *Quart. J. Roy. Meteor. Soc.,* **108,** 739–762.

Trier, S. B., and C. A. Davis, 2007: Mesoscale convective vortices observed during BAMEX. Part II: Influences on secondary deep convection. *Mon. Wea. Rev.,* **135,** 2051–2075.

——, ——, and W. C. Skamarock, 2000: Long-lived mesoconvective vortices and their environment. Part II: Induced thermodynamic destabilization in idealized simulations. *Mon. Wea. Rev.,* **128,** 3396–3412.

Weisman, M. L., 1992: The role of convectively generated rear-inflow jets in the evolution of long-lived mesoconvective systems. *J. Atmos. Sci.,* **49,** 1826–1847.

——, W. C. Skamarock, and J. B. Klemp, 1997: The resolution dependence of explicitly modeled convective systems. *Mon. Wea. Rev.,* **125,** 527–548.